Evaluation of Design Practices in Geotechnical Engineering

Laura Nim Pedersen and Tommy Bank

Structural and Civil Engineering

M.Sc. Thesis

STUDENT REPORT

AALBORG UNIVERSITY

AALBORG UNIVERSITY
STUDENT REPORT

Structural and Civil Engineering
Aalborg University Esbjerg
http://www.aau.dk

Title:
Evaluation of Design Practices in Geotechnical Engineering

Document type:
Master thesis

Project Period:
Fall Semester 2019 and Spring Semester 2020

Project Group:
BM4-6

Participants:
Laura Nim Pedersen
Tommy Bank

Supervisors:
Lars Damkilde

Copies: 1

Number of Pages: 68

Date of Completion:
10/06-2020

Abstract:

The project aims at exploring a possibly untapped potential of soil as a structural material. Rapid developments in computing technology makes e.g. 3D modelling increasingly feasible and facilitates more advanced models. Through numerical analysis the use of a general parametric yield surface, as an alternative to more traditional yield surfaces in geotechnical engineering, is investigated. Shallow foundations of altering geometry are analysed in the commercial finite element software PLAXIS. The general parametric yield criteria will be implemented in the software, as an attempt to simulate the elasto-plastic behaviour of a soil volume more correctly. The parameters used in the analyses are calibrated with experimental data from both compressive and true triaxial tests. In conjunction with the analyses to be performed, the validity of commonly applied assumptions, currently accepted as best practice in the industry, are investigated. Specifically the relations between two and three dimensional analysis, and corrective measures used in practice, are evaluated.

Preface

Present master thesis is conducted on the 3rd and 4th semester of the Master of Science in Structural and Civil Engineering at Aalborg University Esbjerg by Laura Nim Pedersen and Tommy Bank in the period from September 2nd 2019 to June 10th 2020.

The aim of the project is to evaluate well established calculation methods and assumptions in danish geotechnical practice. It is purely a numerical study, performed in PLAXIS, with a primary focus on the bearing capacity of shallow foundations on frictional soil in the ultimate limit state. Two and three dimensional solution techniques are assessed and their discrepancy sought quantified. In continuation of this, a novel yield surface by Professor Lars Damkilde is investigated. Opposed to the traditional Mohr-Coulomb criterion, it is possible to include effects of the intermediate principle stress in the proposed yield surface.

The report is divided in chapters indicated with Y heading, sections indicated with Y.Y heading and subsections indicated with Y.Y.Y heading. Source references are denoted by square brackets; [X]. X being the reference number corresponding to the number in the bibliography at the end of the report. Equations, figures and tables are indicated by (Y, Z), Y being the the chapter number, Z being the equation, figure or table number. Each figure has a caption below the figure, and each table has a caption above the table.

Following software has been utilized during the making of the project; MATLAB R2018a, PLAXIS 2D 2019, PLAXIS 3D 2019, Ipe 7.2.14, Texmaker 5.0.2, SciTE 4.3.3, Microsoft Visual Studio 2019, Intel Parallel Studio XE 2020 with Intel Fortran Compiler 19.1. It should be noted, that Aalborg Universities license for the full version of PLAXIS with VIP functions, unexpectedly ran out during the making of the project and was not renewed. For the better part of the spring 2020 until completion an introductory demo version of PLAXIS was used. User defined soil models and remote scripting is not possible for this version. Furthermore the meshing is limited to 50.000 element.

A special thanks go to the main supervisor Lars Damkilde for guidance and counsel during the project period. Associate Professor Amin Barari and research assistant Francisco Manuel Garcia Rodriguez are thanked for welcoming us as guests for lectures in Aalborg.

Aalborg University Esbjerg, 10/06-2020

Laura Nim Pedersen
lnpe18@student.aau.dk

Tommy Bank
tbank18@student.aau.dk

Nomenclature

Greek letters

α	$\frac{\rho_t}{\rho_c}$ parameter
β	Curvature parameter
Δ	Finite increment
δ	Residual
γ	General specific weight
λ	Plastic multiplier
μ	Slope of yield criterion in the compressive meridian plane
ν	Poisson's ratio
φ	Friction angle
ψ	Dilatancy angle
ρ	Deviatoric stress
σ'_c	Effective uni-axial compressive strength
σ	Standard deviation
σ'_t	Effective uni-axial tensile strength
σ_m	Mean stress
τ	Shear stress
θ	Lode angle
ε_a	Axial strain
ε_V	Volumetric strain

Matrices and Vectors

B	Strain interpolation matrix
D	Elastic constitutive matrix
$\boldsymbol{\varepsilon}$	Strain vector
K	Stiffness matrix
P	Load vector
$\boldsymbol{\sigma}$	Stress vector
$\boldsymbol{\sigma}^*$	Stress vector in transformed coordinate system

Symbols

A_0	Corrected area
′	Apostrophe indicating effective parameters
c	Cohesion
$\overline{c^*}$	ρ_c normalized deviatoric centre of curvature
d	Depth factor
d_s	Relative density
E	Young's modulus
e	Void ratio
E_{oed}	Oedometer modulus
f	Yield criteria
G	Shear modulus
g	Flow rule
i	Inclination factor
I_D	Density index
i,j	Counter variables
K	Bulk modulus
k	Frictional coefficient
K_0	At rest soil pressure coefficient
N	Bearing capacity factor
p	Hydrostatic pressure
q	Surcharge
R	Ultimate bearing capacity
$\bar{r}$	ρ_c normalized radius
s	Shape factor
S_w	Degree of saturation
u,v,w	Displacement coordinates
x,y,z	Cartesian coordinates

Contents

Chapter 1

Introduction

The main focus of present report is to investigate the possibly untapped potential of soil as a structural material. All civil engineering structures are by some means supported by contact with soil and so geotechnical design is always a part of any given project. In conjunction with civil structures becoming larger and availability of natural resources limited, this drives a desire to push designs to the limit. It is expected that the offshore industry will be amongst the frontrunners in developing and implementing new solutions and technology to make advancements within geotechnical structures. With increasing sizes of e.g. wind turbines, where the supporting structures have a large degree of reproducibility, at least within the same project, optimizations can prove very beneficial. The findings can eventually benefit all branches of geotechnical engineering, but designers involved in one off projects such as residential buildings simply do not have the same incentive to drive the development.

Geotechnical engineering is a notoriously experience based field, which to a great extend is justified, considering the unpredictable nature of soils. A downside to this is, in the authors perception, a industry where rules of thumb, that are not necessarily well-document, becomes the norm. This has lead to design practices that can potentially be vastly conservative or result in an actual level of safety below what the designer predicts. A classic example from geotechnical practice in Denmark is a correction of the friction angle when dealing with problems that can be considered as being in a plane strain condition [1]. A case of this was quickly discovered by the authors when reviewing a calculation example of a simple geotechnical problem in a widely used teaching material at the undergraduate level [2]. The bearing capacity of a pad foundation is investigated using well-known bearing capacity formulae with a plane friction angle. This is clearly a three-dimensional problem. Even so a correction on the friction angle is made, which is in accordance with the National Annex of the Eurocode, but does not appear to be particularly judicious.

The non-linear nature of soil as a structural material dictates constitutive models that account for both the elastic and plastic behaviour during loading/unloading. This constitutive relation comprise a yield criterion, which controls whether stress points in a soil domain is in an elastic state or yielding. The ability of a yield criterion to describe the actual physical response of the soil is very much dependent on its complexity and possibilities of obtaining the proper descriptive parameters. Many yield criteria used in practical geotechnical engineering spring from traditional theory presented by e.g. Coulomb (1776) and later on generalised by Mohr (1882) [3].

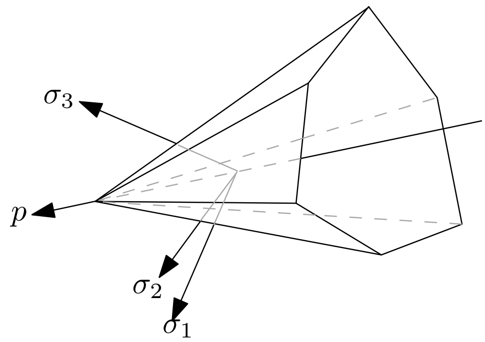

Figure 1.1: Mohr-Coulomb yield surface in principal stress space.

A lot of geostructural analyses is continuously carried out using the Mohr-Coulomb criterion. One of the primary reasons for this is most likely the relatively simple procedure of calibrating the criterion to strength characteristics obtained from experimental results. A pronounced weakness of the Mohr-Coulomb criterion is, that it is generated solely from a compressive friction angle. Thus disregarding the increasing friction angle when approaching a tensile triaxial state. Furthermore, the neglection of the influence of the intermediate principal stress affects the accuracy. The counterpart to this is the Drucker-Prager yield surface (1952) in which all principal stress are equally influential [4]. Though a great number of more or less advanced yield criteria are proposed. Many often suffer from unphysical parameters that can be difficult to quantify and interpret. Adding to this, many criteria are restricted in their application and are only valid for certain materials or types of analysis. This report investigates a general parametric yield surface format proposed by Lars Damkilde, that seeks to encompass a number more traditional yield surfaces whilst being versatile and providing a more precise approximation of the physical phenomena involved. Important capabilities of the proposed yield surface are presented in chapter 3.

Progressive advancements in computer technology pave the way for solving increasingly complex numerical problems. With the possibility of performing a great number of computations within a reasonable time frame, there is an incentive to develop more accurate models. Assumptions and simplifications, which were previously essential to achieve realistic computation durations, might not be as crucial. This could e.g. be analysing three-dimensional problems in a plane strain configuration, being the only viable option at the time. Numerical analyses carried out in this report will to the extend possible be carried out in the commercial finite element software PLAXIS. This is to the authors knowledge by far the most widely used software in the geotechnical industry and hence considered the most relevant. The standard implementation of the Mohr-Coulomb model in PLAXIS will serve as a benchmark for the analysis to be performed.

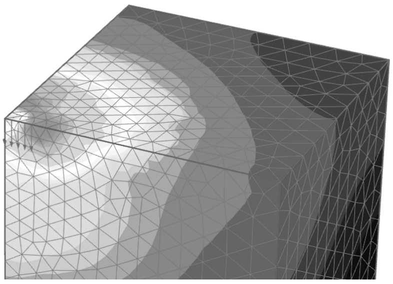

Figure 1.2: Three dimensional finite element mesh.

Project Scope

This thesis aims at investigating the validity of three common design practices for frictional soils in geotechnical engineering stated as

- Analysing structures in plane strain with a increased friction angle
- Analysing structures in axisymmetry with a triaxial friction angle.
- Using the Mohr-Coulomb yield criteria in elasto-plastic finite element analysis.

The influence of the intermediate principal stress and plane strain representation of classical geotechnical problems is scrutinized by analysing long structures of altering proportions in 2D and 3D finite element models. In particular the correction of the friction angle, when treating a problem in plane strain as done in danish practice, is sought quantified, whether this justifies or diminishes the use of it. Traditional bearing capacity formulae serve as a indicative benchmark, to assess the validity of the results obtained. To couple present report with a business that is expected to drive the development within the field, offshore foundations such as circular gravity base are investigated. The validity of common design approaches are examined and compared with both axisymmetric and three-dimensional numerical models. Furthermore, the potential gains, which can be achieved by utilizing a more versatile yield surface, are quantified. The key aspect throughout the studies is the applicability and feasibility of findings in a commercial context. This prescribes coherence between the modelling to be performed and field surveys as well as laboratory tests, involved in determination of soil characteristic.

This thesis is limited to investigating frictional soils. Partly contributed to the fact that the effect of accounting for a tensile friction angle is very pronounced for these materials. The soils used throughout the report are G-12 sand on which Bønding (1977) have performed true triaxial test [5] and Baskarp sand no. 15 where Ibsen (1994) have performed compressive triaxial test [6]. The former contains a large amount of data with individual control over all three principal stresses, but only at failure. The latter have more common triaxial test results, but contains measurements before failure occurs, so that the elastic characteristics can be properly assessed. The Mohr-Coulomb model is put a stake by comparing it to a general parametric yield surface format. This is done on the G-12 sand as this include data on the intermediate principal stress. The General Parametric Yield Surface format is incorporated in PLAXIS as a user-defined material model programmed in Fortran and compiled as a dynamic link library. Performance of the different criteria along with a rating of the complexity involved in setting them up, is evaluated by analysis of a simple shallow foundation. The analyses performed throughout the thesis are written in python language and run in PLAXIS through a remote scripting server, which offers a very effective alternative to simply using the graphical user interface.

Prerequisites

Compression is often taken positive in geotechnical context, but the sign convention used in PLAXIS is adopted throughout this thesis. This being tension positive and compression negative [7]. The ordering of principal stresses throughout the report is $\sigma_1 > \sigma_2 > \sigma_3$. The thesis is limited to ultimate limit state analysis. Even so findings are likely to influence other limit states at a structural level. The elastic behaviour will only be treated to the extend of making for a reasonable estimate of the response. Plastic behaviour, such as hardening, influencing deformations are disregarded for the purposes of this project. All analyses performed are drained and time-independent. Although present report only investigates soils, the principles and models are by no means limited to this material.

Chapter 2

State of the Art

This chapter introduces a number of widely recognized assumptions and design practices in geotechnical engineering. It is important to mention that this is the authors perspective of the status quo. Furthermore, some of the fundamental theory used throughout the thesis is presented for completeness. There is without a doubt both regulatory and internal discrepancies between practitioners throughout the world.

Numerous geotechnical parameters are presented, followed by a short description of a traditional triaxial test procedure to determine the strength of soil. The Mohr-Coulomb yield criteria is described, as this is one of the most extensively used constitutive models for frictional materials. Some widespread solution techniques for solving geotechnical problems are presented. Today and especially historically simplifications allowing three dimensional problems to be solved in a two dimensional framework are essential in geotechnical applications. Therefore plane strain and axisymmetric configurations are presented. Lastly procedures for determining ultimate bearing capacities both analytically and numerically are introduced.

Soil has seemingly endless variations of composition and behaviour, making it incredibly hard to model accurately. Non-linearities may occur at both micro- and macroscopic levels, likewise in both the elastic and plastic regimes [8]. To generate manageable models, simplifications are therefore inevitable. A very essential adaptation for practical geotechnical engineering purposes is to treat soil volumes as continua. This is assessed as being the most viable compromise by e.g. comparing the size of common geotechnical structures to particle sizes of soils. Other approaches, such as modelling soils as discrete particles, is to the authors knowledge not used extensively outside academia. As such this thesis will only model soil with a continuum approach.

2.1 Classification of Soil

In general classification of soil involves a geological assessment and geotechnical classification. The former will not be discussed in this thesis. This section describes various geotechnical parameters to be used when analysing problems in soil. Specific values for the parameters are stated when appropriate throughout the report. Two different sets of test data is used to elucidate the procedures going in to determining the relevant properties of soils. Baskarp sand no. 15 has been for soil testing at Aalborg University for several years. Accordingly the soil is very well described and a considerable amount of test data is available. The primary interest for this thesis is the compressive triaxial tests performed, which is described in 2.1.2. This serves as the basis for describing the conventional procedures in geotechnical design. To comply with the scope of this project, other test types are necessary. Bønding performed true triaxial test on G-12 sand and the results from this study serve as the basis for investigations, where stress states different from compressive triaxial are imperative. The more unconventional testing procedures are described in 3.3.

2.1.1 Geotechnical Parameters

This section goes through the parameters relevant to this study only, as a exhaustive list of parameters in geotechnical engineering would be fierce.

Void ratio defines the ratio between voids and solids in a soil volume, whether the voids are composed of air, water or a combination. As such it can be seen as a measure for how well packed a soil volume is. Generally a relatively low void ratio indicates a dense soil, while a relatively high void ratio indicates loose soil. It is important to mention that void ratios of the same numeric value, does not necessarily imply similar quality. The grading of the soil must be taken into consideration, which motivates another measure as presented in the subsequent paragraph. The void ratio is obviously changed when a soil volume is strained.

Density index is a measure of how the in-situ void ratio compares to a maximum and minimum void ratio determined by standardised testing. It takes on values between 0 and 1, which can be interpreted as a scale ranging from very loose to very dense sediments. This is evident from

$$I_D = \frac{e_{max} - e}{e_{max} - e_{min}} \tag{2.1}$$

where e_{max} represents the loosest possible state of the soil and e_{min} the densest. Regardless of the initial state of the soil it will eventually reach a critical state when stressed sufficiently. This is illustrated in figure 2.1.

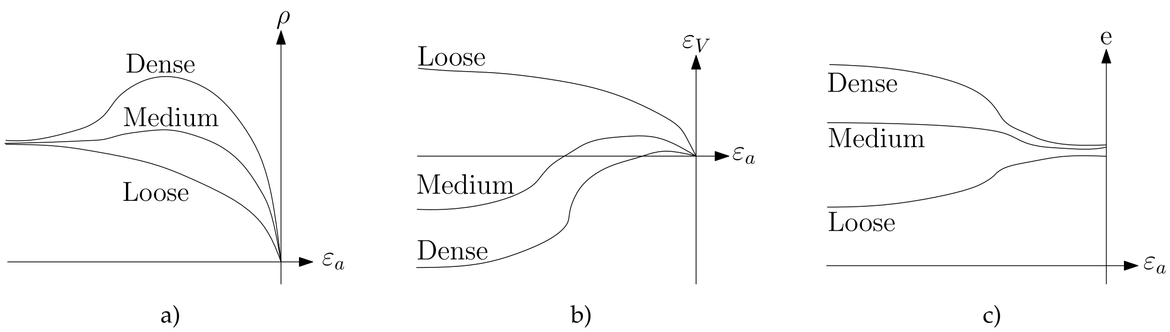

Figure 2.1: Soil behaviour from different density indices.

Loose sediments experience compression until the critical state is reached. Whereas medium and dense sediments experience compression in the beginning and afterwards dilatation will occur. The density index is a good measure to assess what behaviour can be expected from the soil being analysed. As the illustration in figure 2.1 indicates it could improve accuracy to include a plastic strain softening measure for dense sand. This is not accounted for in perfect plasticity and so the initial void ratio used in analysis does not influence the ultimate bearing capacity. There is no explicit definition for when a soil is loose or dense, and so throughout this thesis the terminology for the two soil types investigated will be as shown in table 2.1. Fittingly these tests are both performed on three levels of compaction.

Table 2.1: Soil compactness.

Material	Loose	Medium	Dense		
Baskarp sand no. 15	$I_D = 0.01$	$I_D = 0.51$	$I_D = 0.80$	$e_{min} = 0.549$	$e_{max} = 0.858$
G-12 sand	$I_D = 0.29$	$I_D = 0.68$	$I_D = 0.88$	$e_{min} = 0.510$	$e_{max} = 0.850$

Specific weight and density may refer to a number of quantities in geotechnics. The conventional nomenclature for these is listed in table 2.2.

Table 2.2: Density and specific weight.

Parameter		Description
γ	$[^{kN}/_{m^3}]$	General specific weight
γ_d	$[^{kN}/_{m^3}]$	Specific weight for dry soil
γ_w	$[^{kN}/_{m^3}]$	Specific weight for water
γ_m	$[^{kN}/_{m^3}]$	Specific weight for fully saturated soil
$\gamma' = \gamma_m - \gamma_w$	$[^{kN}/_{m^3}]$	Reduced specific weight
γ_s	$[^{kN}/_{m^3}]$	Specific weight for solids
$d_s = {}^{\gamma_s}/_{\gamma_w}$	$[-]$	Relative density

The general specific weight is determined as

$$\gamma = \frac{d_s + eS_w}{1+e} \cdot \gamma_w \tag{2.2}$$

where e is the void ratio and S_w is the soil's degree of saturation. As in many disciplines the specific weight of water is usually set equal to 10 $^{kN}/_{m^3}$. The fully saturated specific weight can be found by setting the degree of saturation equal to one and equal to zero to find the dry specific weight. For frictional soils a relative density of around 2.65 is quite common [3, p. 28]. This is confirmed by the soil samples used which are determined as 2.64 and 2.65 through preparatory tests.

Poisson's ratio is the well-known measure of expansion or contraction perpendicular a stressed surface in a solid. In soils this parameter is by no means a constant. Many frictional soils may experience contractive volume strains at lower stress level followed by dilative behaviour when the load is increased [6]. A number of other factors, such as undrained behaviour, may also dictate the properties of the poisson's ratio used for analysis of problems in soil. For the relatively simple structures and load cases investigated in this thesis, it is thought sufficient to simplify the matter. Typically frictional soils will be in the range of 0.1 to 0.4 [9]. For offshore structures, if not determined in other ways, Poisson's ratio is often assumed to be equal to 0.3 for coarse soil as sand, which is used in this project [10].

Stiffness modulus in soil has a large degree of variability. It is susceptible to changes depended on the stress level and history, which may stem from external loads or merely the variation in confining pressure with depth. For linear elastic models this will inevitably result in a compromise where the stiffness will be over- or underestimated. If using the initial tangent modulus the stiffness will in most cases deviate from the real behaviour almost immediately and underpredict strains significantly.For the purposes of this study a secant modulus at 50% strength is utilized as Young's modulus. This is quite common for problems involving loading of soils. Unloading and reloading problems will often behave somewhat stiffer. Alternative stiffness moduli are often used in geotechnical calculations, depending on the test procedure. It is possible to use these in the Mohr-Coulomb model in PLAXIS, where the relationship between these and Young's modulus is defined by Hooke's law.

The shear modulus is given by

$$G = \frac{E}{2(1+\nu)} \tag{2.3}$$

The Bulk modulus is given by

$$K = \frac{E}{3(1-2\nu)} \tag{2.4}$$

The Oedometer modulus is given by

$$E_{oed} = \frac{(1-\nu)E}{(1-2\nu)(1+\nu)} \tag{2.5}$$

Cohesion is one of two major contributors to how shear strength of soil is traditionally assessed. It is the stress independent term denoted c in Mohr-Coulomb's failure criterion, which is presented in section 2.2.1. In the context of this study only the effective cohesion, c', is of interest. A common rule of thumb in danish geotechnical practice for friction angle is to assume no cohesion for frictional soil. This is undoubtedly a safe assumption, but also justified. Even coarse grained sands can exhibit an apparent cohesion from testing, which might not be physically reasonable. Coarse grained soil may be cohesive when moist, but not when either dry or saturated. The potential pitfalls from this is exemplified through classical bearing capacity formulae in section 2.3.2.

Friction angle is the second parameter contributing to the shear strength. This is the stress dependent term in Mohr-Coulomb's failure criterion and denoted φ. It is also called the internal angle of friction. As for the cohesion, only the effective friction angle, φ', is used. It is widely recognized, and has been for more than a century, that the friction angle is stress dependent [11]. Even so a linearised angle is still used extensively, due to its simplicity. This is elucidated in reviewing the Mohr-Coulomb criterion in section 2.2.1.

Both the cohesion and the friction angle is conventionally found from triaxial tests. The friction angle obtained from such tests is denoted φ'_{tr}. It obviously stems from a very specific stress state and so may not be applicable to all solution techniques in geotechnical problems. A clear-cut example of this is analysis performed in a plane strain configuration, where the stress state deviates from triaxial condition. Comparison of test results from triaxial and biaxial experiments have indicated a apparent increase in friction angle for plane problems [3]. In Denmark this is traditionally accounted for by increasing the friction angle obtained from triaxial testing, thus introducing what is known as a plane friction angle, φ'_{pl}. For many years this was done by simply increasing φ'_{tr} by 10%. This still serves as the upper limit for the increase, which is determined in terms of the density index as given by

$$\varphi'_{pl} = min \left\{ \begin{matrix} 1.1\varphi'_{tr} \\ \varphi'_{tr}(1 + 0.163 I_D) \end{matrix} \right\} \tag{2.6}$$

The increase of friction angle has a potentially huge impact on the ultimate bearing capacity of a geotechnical structure. This motivates a scrutinization of this seemingly rather crude relationship and further poses the question, when is plane strain a valid assumption.

Dilatancy angle can be viewed as a measure of how the volume of soils will behave during failure, denoted ψ. In layman terms it can be expressed as how much interlocking grains must "lift" to pass each other, which it of course must, for failure to occur. From this it is easy to imagine that densely compacted grains must overcome a relatively steep "climb", whereas loosely packed sidements might succumb with more ease.

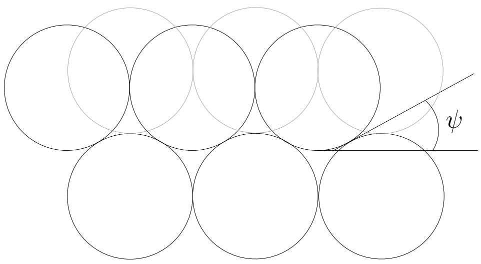

Figure 2.2: Interpretation of dilatancy angle.

It is common to use a constant dilatancy angle when modelling soil, although this deviate from the real behaviour. The quantity is often found by a simple relation with the friction angle [12]

$$\psi = \phi - 30 \tag{2.7}$$

This, to the authors knowledge, generally predicts a lower angle than what can be measured from testing. The angle can be approximated from a linearisation of the axial and volumetric strains in a conventional triaxial test, as illustrated below.

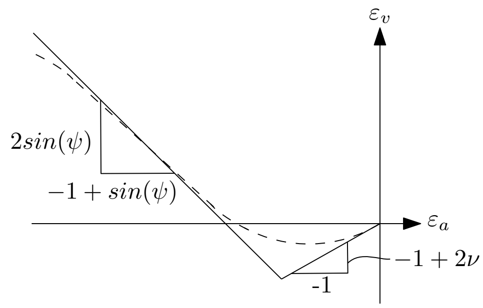

Figure 2.3: Determination of dilatancy angle.

From this it is seen that the dilatancy angle can be determined as [13] shown in equation 2.8.

$$\psi = sin^{-1}\left(\frac{\frac{d\varepsilon_V}{d\varepsilon_a}}{\frac{d\varepsilon_V}{d\varepsilon_a} - 2}\right) \tag{2.8}$$

2.1.2 Conventional Soil Testing

In attempt to find the strength of a given soil test, a widely recognized procedure is conducting a compressive triaxial test. This is a fundamental test in soil mechanics, described in present section.

A cylindrical soil test is exposed to an axisymmetrical stress condition. The stresses are ranked with the vertical stress being the largest compressive principal stress and the horizontal stresses being the smallest. In a compressive triaxial test the intermediate principal stress coincide with the latter, as depicted in figure 2.4.

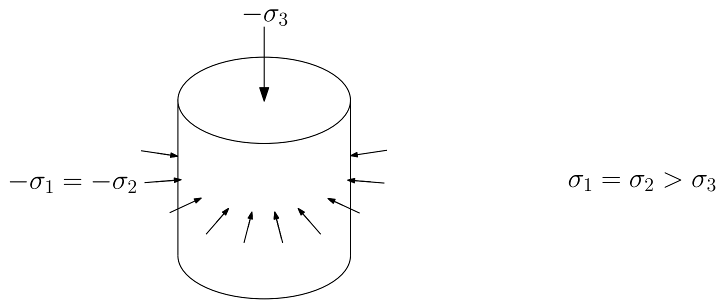

Figure 2.4: Principle of compressive triaxial test.

The test is put in a chamber between two plates at the top and bottom, the upper being a pressure head. The plates are stiff and ideally smooth by applying rubber membranes with silicone in between, to avoid inexpedient deformations. The test is put under an isotropic constant pressure via fluid inside the chamber. The tests are set up with different chamber pressures to mimic different in-situ stresses. A stress increase is made by the pressure head and the deviator stress is determined as the applied load, P, on the top surface, A, of the soil test presented in equation 2.9.

$$\sigma_3 - \sigma_1 = \frac{P}{A} \tag{2.9}$$

The soil test experience relatively large deformations and the top surface expands, assuming that the soil test remain cylindrical under compression. To account for this a corrected area of the top surface, used to find the deviator stress at a specific stress condition, is formulated. The corrected area is calculated based on the area without load, A_0, the volume strain, ε_V, measured by the water squeezed out of the soil test, and the vertical strain, ε_a, measured directly by the vertical deformation of the soil test. Calculation of the corrected area is presented in equation 2.10.

$$A = A_0 \frac{1-\varepsilon_V}{1-\varepsilon_a} \tag{2.10}$$

Rewriting equation 2.9 in terms of equation 2.10 the deviatoric stress is determined as

$$\sigma_3 - \sigma_1 = \frac{P(1-\varepsilon_a)}{A_0(1-\varepsilon_V)} \tag{2.11}$$

By gradually applying load and collecting data until the soil sample fails, it is possible to obtain both elastic and strength characteristics. The results are often presented as in figures 2.1a and 2.1b.

2.2 Elasto-Plastic Constitutive Modelling

In an attempt to simulate the real soil behaviour in a feasible manor, an elasto-plastic framework is somewhat indispensable in geotechnical engineering. The constitutive models formed from such a framework are plentiful and of varying complexity. To keep this study concise, only relatively simple elasto-plastic concepts and models are investigated. This implies that well-documented or physically justified formulations are key. A commonly accepted idealisation for modelling soils is to assume a linear elastic perfectly plastic solid. This implies that the loading and re-loading path have the same slope, as in the one-dimensional example in figure 2.5. The approximation is often accompanied by an assumption of homogeneity and isotropy.

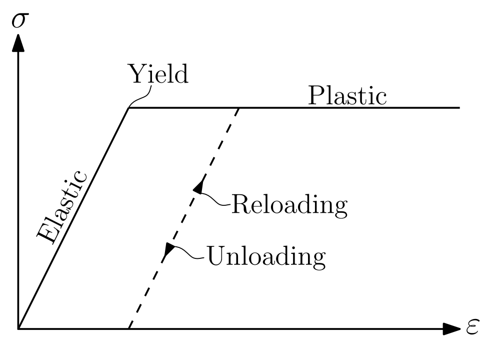

Figure 2.5: Linear elastic perfectly plastic stress-strain relation.

A linear elastic perfectly plastic material model contain the following three basic elements [8]:

- A law defining the elastic stress-strain relationship.
- A yield criterion initializing plastic flow, denoted f.

- A plastic flow rule defining plastic stress-strain relationship, denoted g.

This can also be extended to include a hardening law, where e.g. strength parameters vary with the plastic strains. This will obviously invalidate the assumption of perfect plasticity.

The linear elastic stress-strain relation is often given by the generalized hooke's law [14], expressed in cartesian coordinates in equation 2.12. This could also be a anisotropic or non-linear elastic law, but that is outside the scope of this thesis.

$$\begin{Bmatrix} \Delta\sigma'_{xx} \\ \Delta\sigma'_{yy} \\ \Delta\sigma'_{zz} \\ \Delta\tau_{xy} \\ \Delta\tau_{xz} \\ \Delta\tau_{zy} \end{Bmatrix} = \frac{E'}{(1+\nu')(1-2\nu')} \begin{bmatrix} 1-\nu' & \nu' & \nu' & 0 & 0 & 0 \\ \nu' & 1-\nu' & \nu' & 0 & 0 & 0 \\ \nu' & \nu' & 1-\nu' & 0 & 0 & 0 \\ 0 & 0 & 0 & \frac{1}{2}(1-2\nu') & 0 & 0 \\ 0 & 0 & 0 & 0 & \frac{1}{2}(1-2\nu') & 0 \\ 0 & 0 & 0 & 0 & 0 & \frac{1}{2}(1-2\nu') \end{bmatrix} \begin{Bmatrix} \Delta\varepsilon_{xx} \\ \Delta\varepsilon_{yy} \\ \Delta\varepsilon_{zz} \\ \Delta\gamma_{xy} \\ \Delta\gamma_{xz} \\ \Delta\gamma_{zy} \end{Bmatrix} \tag{2.12}$$

A yield criterion defines whether a material is in a elastic or plastic state, see figure 2.6. In a multi-axial stress state a yield criterion can be visualized as a surface in principal stress space. After yielding the stresses rearrange whilst the strains can still increase. In the case of linear elastic perfectly plastic behaviour, no material fracture is modelled and so strains can in principle increase indefinitely at the material level. At a structural level some plasticity will develop locally even at low load levels, but the adjacent zones may still be in an elastic state. Here failure occurs when an entire surface is in a plastic state and a uncontrollable mechanisms forms.

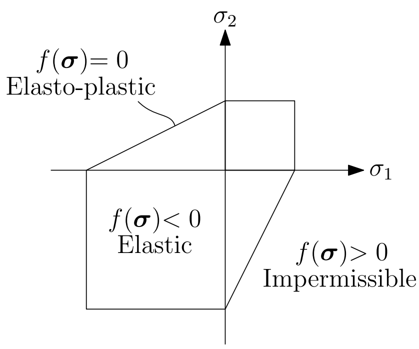

Figure 2.6: Yield function.

A flow rule, also known as plastic potential, dictates the direction of plastic strains after yielding has occurred. Overall there are two types of flow; associated and non-associated. In general the real behaviour of soil obey to non-associated flow. Even so, associated flow is often assumed, amongst other things to avoid some difficulties in solving numerical problems with a non-associated flow rule. Associated flow is also the assumption throughout this report. This prescribes a potential surface which equals the yield surface. In other words, the plastic strain increments are co-directional with the normal to the yield surface. This is known as the normality condition. In using such an assumption for soils, it is necessary to make corrections on the parameters used to generate the yield surface and plastic potential surface. This is exemplified in figure 2.7.

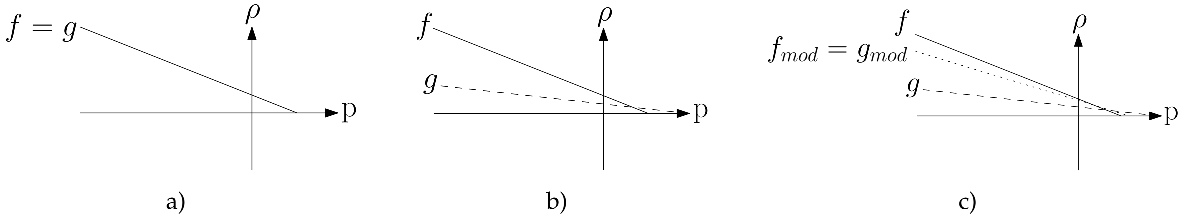

Figure 2.7: Yield surface and plastic potential in meridian plane.

If the plastic potential was simply put equal to the yield surface without corrections, it would overestimate dilatancy. Numerous studies show that increase in the dilatancy angle causes a considerable increase in the ultimate bearing capacity [15]. To bypass this, a modification to the strength parameters was proposed by Davis (1968). This leads to a reduction of the friction angle and cohesion. The dilatancy angle is set equal to the modified friction angle, thus obeying the theory of associated plasticity. The modified friction angle and cohesion is given by

$$\varphi'_{mod} = tan^{-1}\left(\frac{sin(\varphi')cos(\psi)}{1 - sin(\varphi')sin(\psi)}\right) \quad \wedge \quad c'_{mod} = c'\left(\frac{cos(\varphi')cos(\psi)}{1 - sin(\varphi')sin(\psi)}\right) \tag{2.13}$$

known as Davis formula [16]. The parameters to be used in analysis with associated flow is as stated below for clarification.

$$c'_{mod} \quad \wedge \quad \varphi'_{mod} \quad \wedge \quad \psi_{mod} = \varphi'_{mod} \tag{2.14}$$

Elasto-plastic refers to material behaviour that is either purely elastic or a combination of purely elastic and purely plastic components. When a soil volume is subjected to notable loading it will undergo both elastic and plastic strains. In other words some strains are reversible and some are irreversible. This means there is no unique relationship between stresses and total strains once yielding occurs and so the constitutive stress-strain relation is expressed in incremental form [14].

$$\Delta\boldsymbol{\sigma}' = \boldsymbol{D}'_{ep}\Delta\boldsymbol{\varepsilon} \tag{2.15}$$

Here stated for effective stresses and with the constitutive matrix dependent on the stress state and history. The total strain increment is composed of elastic and plastic components.

$$\Delta\boldsymbol{\varepsilon} = \Delta\boldsymbol{\varepsilon}^e + \Delta\boldsymbol{\varepsilon}^p \tag{2.16}$$

The stress increment can be determined from the elastic strains and the elastic constitutive matrix

$$\Delta\boldsymbol{\sigma} = \boldsymbol{D}'\Delta\boldsymbol{\varepsilon}^e \tag{2.17}$$

Combining equation 2.16 and 2.17, the stress increment is given by the total and plastic strain increments.

$$\Delta\boldsymbol{\sigma} = \boldsymbol{D}'(\Delta\boldsymbol{\varepsilon} - \Delta\boldsymbol{\varepsilon}^p) \tag{2.18}$$

The plastic strain increment is defined from the flow rule with a plastic multiplier.

$$\Delta\varepsilon^p = \Delta\lambda \frac{\partial g}{\partial \sigma} \tag{2.19}$$

Turning towards more specific procedures used in PLAXIS, the actual stress state is found at step i in an incremental process as

$$\boldsymbol{\sigma}^i = \boldsymbol{\sigma}^{i-1} + \Delta\boldsymbol{\sigma} \quad where \quad \Delta\boldsymbol{\sigma} = \boldsymbol{D}'\Delta\varepsilon - \Delta\lambda \boldsymbol{D}' \frac{\partial g}{\partial \boldsymbol{\sigma}} \tag{2.20}$$

When the soil is in a plastic stress state is must satisfy the yield criterion $f(\boldsymbol{\sigma} + \Delta\boldsymbol{\sigma}) = 0$ and consequently also its derivative. This is known as the consistency equation

$$\left(\frac{\partial f}{\partial \boldsymbol{\sigma}}\right)^T \Delta\boldsymbol{\sigma} = 0 \tag{2.21}$$

Substituting 2.20 into 2.21 the plastic multiplier can be isolated

$$\Delta\lambda = \frac{\left(\frac{\partial f}{\partial \sigma}\right)^T \boldsymbol{D}'\Delta\boldsymbol{\varepsilon}}{\left(\frac{\partial f}{\partial \sigma}\right)^T \boldsymbol{D}' \left(\frac{\partial g}{\partial \sigma}\right)} \tag{2.22}$$

2.2.1 The Mohr-Coulomb Model

This section describes the Mohr-Coulomb yield criterion in its basic form and addresses the specifics towards its implementation in PLAXIS. The Mohr-Coulomb model refers to "the linear elastic perfectly plastic model with Mohr-Coulomb failure criterion" [9]. There are more advanced soil models in PLAXIS, where features are added or replaces parts of the Mohr-Coulomb model. The Hardening Soil model with small-strain stiffness is an example which, with the Mohr-Coulomb model as the basis, accounts for more effects as the names implies.

The Mohr-Coulomb yield criterion is till this day, in spite of more or less obvious shortcomings, still used to a great extend by practitioners in the geotechnical society. The criterion, as it is known today, is formulated from the major and minor principal stress, thus disregarding the intermediate principal stress. This facilitates a relatively simple calibration procedure from conventional compressive triaxial tests. This is a huge contributor to the criterion's popularity.

The Mohr-Coulomb criterion is in modern tongue a hybrid. It stems from two criteria, namely the Coulumb failure criterion (1776) and the Mohr criterion (1900) [4]. Starting with the former, and without going into the history behind it, Coulomb suggested that soils exhibited stress-independent and stress-dependent strength parameters. Namely cohesion and friction angle. By plotting test results in a $\sigma - \tau$ diagram, probably from the likes of a direct shear test, he formulated the Coulomb failure criterion. This proposes a straight line, through stresses at failure obtained from tests, which defines when a material is yielding as shown in figure 2.8.

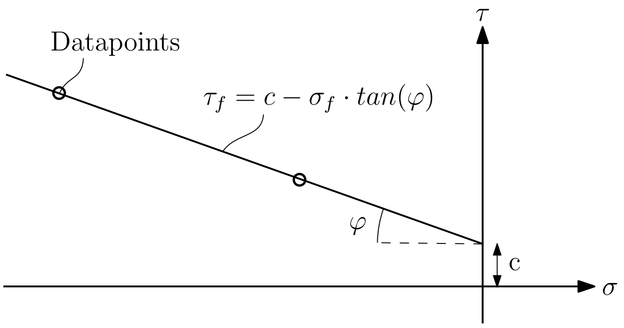

Figure 2.8: Coulomb failure criterion found by datapoints from shear strength tests.

Here τ_f is the shear stress and σ_f is the normal stress, on the failure plane. The material parameter c represent the cohesion and is defined from the intersect with the τ-axis. φ is the friction angle and is defined as the slope of the tangent line. From this it is clear that the friction contribution to the shear strength is proportional with the normal stress. It was later discovered by Terzaghi (1925) [17] convenient to analyse soils in terms of effective stresses, in which Coulombs failure criterion reads:

$$\tau_f = c' - \sigma_f' tan(\varphi') \tag{2.23}$$

Mohr suggested that failure was a arbitrary function dependent on the normal stress on a plane. Visually this can be represented as a tangent line to Mohr's circles of stress, with the limitation that no part of the circles can extend beyond the line, as seen in figure 2.9.

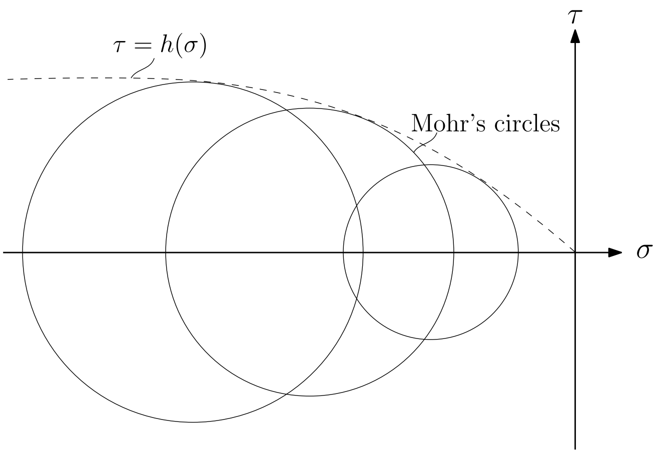

Figure 2.9: Mohr failure criterion; a non-linear envelope tangent to Mohr's circles.

Although the origin of the combination of the criteria is unknown, it still serves as a persisting and well-renowned yield criterion for frictional and cohesive materials. The hybrid is popularly known as the Mohr-Coulomb criterion. Simply put, it can be seen as a idealised linear tangent fit to Mohr's circles, see figure 2.10.

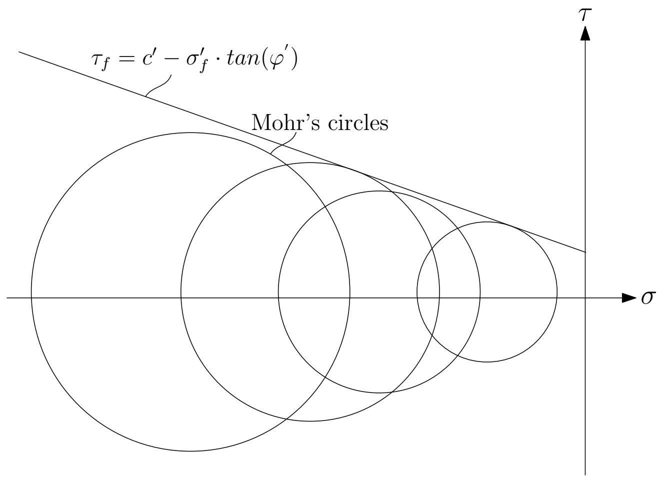

Figure 2.10: Mohr-Coulomb failure criterion.

In a modern day context the yield criterion is traditionally fitted to effective principal stresses resulting from compressive triaxial testing at varying confining pressures. The fitting procedure is explained further in section 4.3.1. Expressing τ_f and σ'_f in terms of principal stresses as shown in figure 2.11

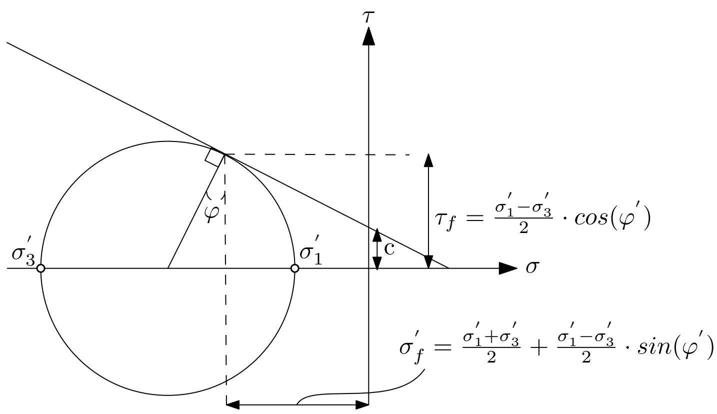

Figure 2.11: Mohr-Coulomb from principal stresses.

from which the yield criterion can be formulated as

$$f(\sigma'_1, \sigma'_3) = 2c' cos(\varphi') - (\sigma'_1 + \sigma'_3) sin(\varphi') - (\sigma'_1 - \sigma'_3) \tag{2.24}$$

Bearing in mind the conventional ordering of principal stresses $\sigma'_1 \geq \sigma'_2 \geq \sigma'_3$, the uni-axial compressive and tensile strength from $f(0, \sigma'_c) = 0$ and $f(\sigma'_t, 0) = 0$ respectively, can be found.

$$\sigma_c = \frac{2c cos(\varphi')}{1 - sin(\varphi')} \quad \wedge \quad \sigma_t = \frac{2c cos(\varphi')}{1 + sin(\varphi')} \tag{2.25}$$

Another often used and elegant form of the criterion in terms of principal stresses read

$$f(\sigma'_1, \sigma'_3) = k' \sigma'_1 - \sigma'_3 - \sigma'_c \tag{2.26}$$

where the frictional coefficient, k, and the uni-axial compressive strength, σ_c, is given by

$$k' = \frac{1+sin(\varphi')}{1-sin(\varphi')} \quad \wedge \quad \sigma'_c = 2c'\sqrt{k'} \tag{2.27}$$

This visualizes as follows in the σ_1-σ_3 plane

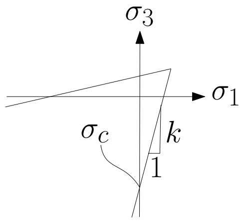

Figure 2.12: k and σ_c in σ_1-σ_3 plane.

In three dimensional principal stress space the Mohr-Coulomb criterion visualises as a surface comprised of six linear segments. These each represent altering ordering of the principal stresses. As such, formulating the entire yield surface ensures independence towards the ordering of principal stresses. Graphically the yield surface, depending on its strength parameters, resembles figure 2.13 in the principle stress space, deviatoric plane and meridian plane.

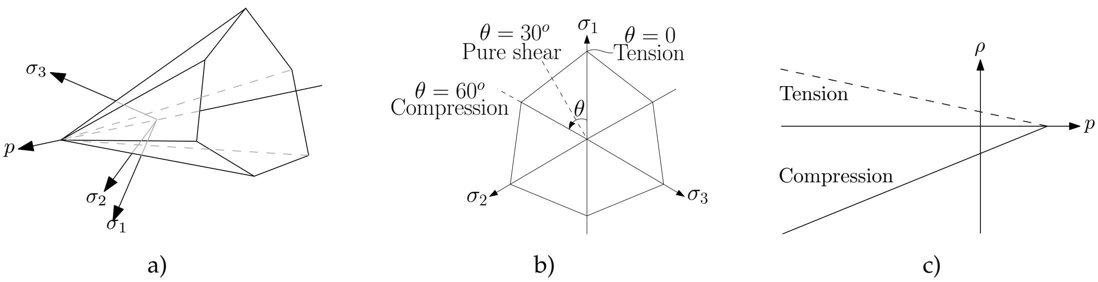

Figure 2.13: Mohr Coulomb yield surface presented in a) Principle stress space b) Deviatoric plane c) Meridian plane.

The yield surface described by the Mohr-Coulomb yield criterion has a fixed ρ_t/ρ_c ratio, proportional to the friction angle, see figure 2.14. It is convenient to establish this ratio from a Mohr-Coulomb criterion in Haigh-Westergaard coordinates [18]

$$f(p,\rho,\theta) = \sqrt{2}psin(\varphi') + \sqrt{3}\rho sin\left(\theta + \frac{\pi}{3}\right) + \rho cos\left(\theta + \frac{\pi}{3}\right) sin(\varphi') - \sqrt{6}ccos(\varphi') \tag{2.28}$$

where p is the hydrostatic pressure, ρ is the deviatoric stress and θ is the lode angle. The deviatoric stress at yielding for uni-axial tension and compression in the π-plane can be found from $f(0,\rho_t,0) = 0$ and $f(0,\rho_c,\frac{\pi}{3}) = 0$. By substituting c with the expression from equation 2.25 the deviator stresses are found as

$$\rho_t = \frac{\sqrt{6}\sigma'_c(1-sin(\varphi'))}{3+sin(\varphi')} \quad \wedge \quad \rho_c = \frac{\sqrt{6}\sigma'_c(1-sin(\varphi'))}{3-sin(\varphi')} \tag{2.29}$$

in terms of the uni-axial compressive strength. From this the ratio between the two quantities can be established.

$$\frac{\rho_t}{\rho_c} = \frac{3 - sin(\varphi')}{3 + sin(\varphi')} \tag{2.30}$$

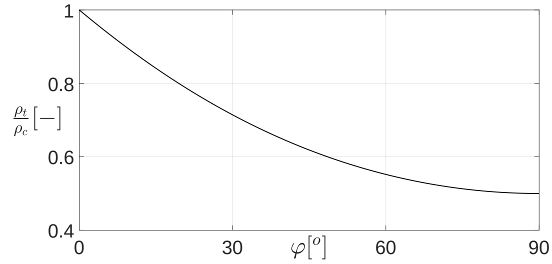

Figure 2.14: ρ_t/ρ_c ratio for friction angles ranging from Tresca to Rankine.

The difference between the triaxial compression and extension extrema can be further clarified from inspecting Mohr's failure mode criterion. This postulate that there are two possible failure planes which forms the angle β with the largest principal stress, as visualised in figure 2.15. This shows a classic failure mechanics under a footing.

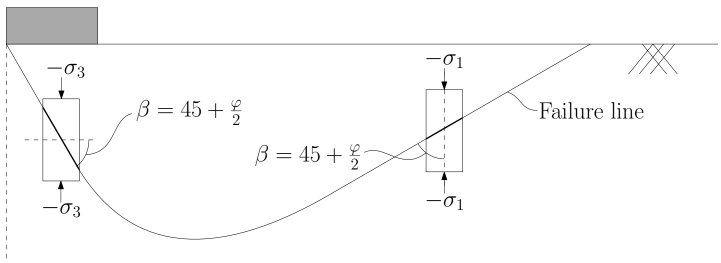

Figure 2.15: Failure planes for triaxial compression (left) and extension (right).

The Mohr-Coulomb Model in PLAXIS consist of five basic parameters and an optional sixth if tension cut-off is used.

Table 2.3: Basic parameters in the Mohr-Coulomb model.

Parameter		Description
E	$[kN/m^2]$	Young's modulus
ν	$[-]$	Poisson's ratio
c	$[kN/m^2]$	Cohesion
φ	$[^o]$	Friction angle
ψ	$[^o]$	Dilatancy angle
σ_t	$[kN/m^2]$	Uni-axial tensile strength

The linear elastic part of the Mohr-Coulomb model is based on Hooke's law as given in equation 2.12. The perfectly plastic part of the model obey the Mohr-Coulomb yield criterion. It is formulated as in equation 2.24 with altering orders of principal stresses to form a total of six segments. The flow rule implemented is non-associated with a form similar to the yield surface. It reads

$$g = \frac{1}{2}(\sigma_1' - \sigma_3') + \frac{1}{2}(\sigma_1' + \sigma_3')sin(\psi) \leq 0 \tag{2.31}$$

and like the yield surface is formulated for six segments, with alternating order of principal stresses [9]. If tension cut-off is used, this is simply modelled as a restriction on the principal stresses to take any positive value in its default setting. It is though possible to define a allowable tensile stress, σ_t.

$$f_4 = \sigma_1' - \sigma_t \leq 0 \quad \wedge \quad f_5 = \sigma_2' - \sigma_t \leq 0 \quad \wedge \quad f_6 = \sigma_3' - \sigma_t \leq 0 \tag{2.32}$$

2.3 Solution Techniques

This section presents the solution techniques for geotechnical problems used in this thesis. This is by no means an exhaustive list, but offers some insight to both the simplicity and complexity that calls for a deliberate approach to the problem at hand. Besides the procedures explicitly stated in this section, the program "ABC - Analysis of Bearing Capacity Version 1.0 Build 1" developed by Martin (2004) is used for benchmarking. In short, this uses the method of stress characteristics in a finite difference scheme to solve classical bearing capacity problems. For further details see [19].

2.3.1 Plane Strain and Axisymmetry

Plane strain is often assumed for geotechnical structures that are significantly larger in one dimension, compared the two other. Tunnels, strip footings, retaining walls and breakwaters are cases of structures which often exhibit such geometric characteristics. These problems can be solved in a plane strain configuration, provided that not only the geometry, but also the loading is continuous. Figure 2.16 illustrates an example in cartesian coordinates, where the structure is much longer in the z-direction compared to the x- and y-direction.

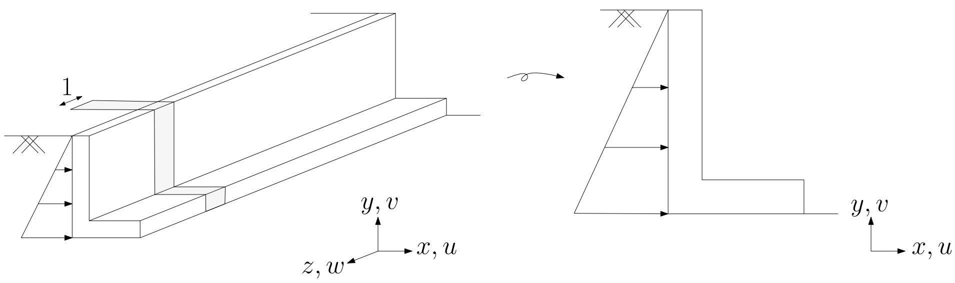

Figure 2.16: Plane strain example.

The displacement out of plane relative to those in the x-y plane is close to zero, as adjacent material constrains it. This leads to the assumption of $w = 0$. Furthermore the u and v displacements are considered independent of the z-coordinate. This leads to the following strains being set equal to zero.

$$\varepsilon_{zz} = \frac{\partial w}{\partial z} = 0 \quad \wedge \quad \gamma_{yz} = \frac{\partial w}{\partial y} + \frac{\partial v}{\partial z} = 0 \quad \wedge \quad \gamma_{xz} = \frac{\partial w}{\partial x} + \frac{\partial u}{\partial z} = 0 \tag{2.33}$$

This ultimately reduces the size of the problem considerably, resulting in the constitutive relation being formulated as below.

$$\begin{Bmatrix} \Delta\sigma'_{xx} \\ \Delta\sigma'_{yy} \\ \Delta\sigma'_{zz} \\ \Delta\tau'_{xy} \end{Bmatrix} = \begin{bmatrix} D'_{11} & D'_{12} & D'_{13} & D'_{14} \\ D'_{21} & D'_{22} & D'_{23} & D'_{24} \\ D'_{31} & D'_{32} & D'_{33} & D'_{34} \\ D'_{41} & D'_{42} & D'_{43} & D'_{44} \end{bmatrix} \begin{Bmatrix} \Delta\varepsilon_{xx} \\ \Delta\varepsilon_{yy} \\ 0 \\ \Delta\gamma_{xy} \end{Bmatrix} \tag{2.34}$$

It is common to temporarily exclude $\Delta\sigma_{zz}$. This simplifies to a two-dimensional problem. It should be noted that non-zero entries of the material matrix must be independent of the out-of-plane stress.

Axisymmetry can be utilized for structures that possess rotational symmetry. Examples of these include circular footing, circular piles and cylindrical triaxial tests. The latter is of course not a structure as such, but still a good example. Much like in the plane strain configuration the loading must be uniform or alternatively centrally placed. An example in cylindrical coordinates is shown in figure 2.17.

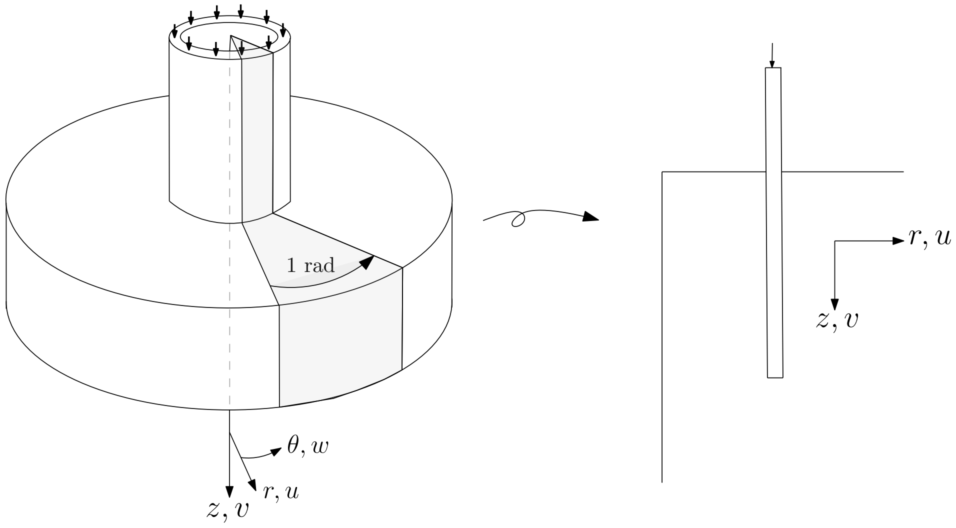

Figure 2.17: Axisymmetric example.

Due to symmetry displacements in the θ-direction are zero and displacements in the r and z directions independent of θ. This leads to the following zero strains.

$$\gamma_{r\theta} = \frac{1}{r}\frac{\partial u}{\partial \theta} + \frac{\partial w}{\partial r} - \frac{w}{r} = 0 \quad \wedge \quad \gamma_{z\theta} = \frac{\partial w}{\partial z} + \frac{1}{r}\frac{\partial v}{\partial \theta} = 0 \tag{2.35}$$

As exemplified in the above it is usual to use cylindrical coordinates for such problems. This leads to the following reduced constitutive relation.

$$\begin{Bmatrix} \Delta\sigma'_{r} \\ \Delta\sigma'_{z} \\ \Delta\sigma'_{\theta} \\ \Delta\tau'_{rz} \end{Bmatrix} = \begin{bmatrix} D'_{11} & D'_{12} & D'_{13} & D'_{14} \\ D'_{21} & D'_{22} & D'_{23} & D'_{24} \\ D'_{31} & D'_{32} & D'_{33} & D'_{34} \\ D'_{41} & D'_{42} & D'_{43} & D'_{44} \end{bmatrix} \begin{Bmatrix} \Delta\varepsilon_{r} \\ \Delta\varepsilon_{z} \\ \Delta\varepsilon_{\theta} \\ \Delta\gamma_{rz} \end{Bmatrix} \tag{2.36}$$

2.3.2 Bearing Capacity Formulae

For the footings investigated, classical and well-renowned bearing capacity formula serve as a indicative measure to assess the results. A lot of the formulae still in use worldwide stem from Terzaghi's (1943) work [3]. It is based on the assumption of superposition of three contributions to the resistance of a infinitely long strip footing. The soil is a Mohr-Coulomb soil with a cohesion, friction angle and specific weight. Furthermore, a perfectly rough footing is assumed implying that the friction angle between the base and the soil coincides with the friction angle of the soil itself. Terzaghi's bearing capacity equation in the general case is not exact, but conservative. In its basic form Terzaghi's bearing capacity reads

$$R = R_\gamma + R_q + R_c = \frac{1}{2}\gamma b^2 N_\gamma + qbN_q + cbN_c \tag{2.37}$$

In danish geotechnical practice a modified version of the bearing capacity formula by Brinch-Hansen (1970) is used

$$\frac{R'}{A'} = \frac{1}{2}\gamma' b' N_\gamma s_\gamma i_\gamma + q' N_q s_q i_q d_q + c' N_c s_c i_c d_c \tag{2.38}$$

The ultimate limit load is the sum of the three contributions related to the cohesion, surcharge and specific weight. The bearing capacity factors N_γ, N_q and N_c are solely based on the friction angle of the soil for drained conditions. The expressions for the bearing capacity factors assume the soil to be a perfectly plastic material obeying an associated flow rule with the friction angle equal to the dilation angle. N_q and N_c have exact plasticity solutions based on closed-form expressions by Prandtl (1921) and Reissner (1924) under the assumption of an associated flow rule for the material [3].

$$N_q = \frac{1 + sin(\varphi)}{1 - sin(\varphi)} e^{\pi tan(\varphi)} \quad \wedge \quad N_c = \frac{N_q - 1}{tan(\varphi)} \tag{2.39}$$

N_γ on the other hand has been subject to many suggestions and alterations throughout history. In the norms and literature of today there are still a number of different expressions, some of which is listed below in table 2.4.

Table 2.4: Bearing capacity factor N_γ.

Source	N_γ
Eurocode 7 [10]	$2(N_q - 1)tan(\varphi)$
Eurocode 7, DKNA [1]	$\frac{1}{4}((N_q - 1)cos(\varphi))^{\frac{3}{2}}$
DNV no. 30.4 [20]	$1.5(N_q - 1)tan(\varphi)$
Martin, 2005 [21]	Numerical solution

The numerical discrepancy between them is illustrated in figure 2.18.

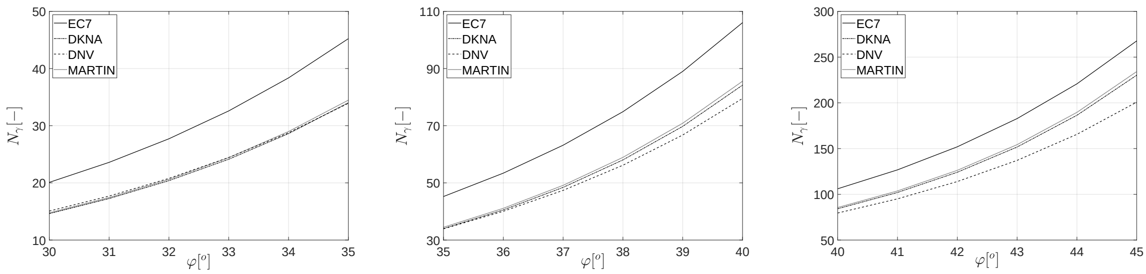

a) b) c)

Figure 2.18: Bearing capacity factor N_γ as function of friction angle.

To put this in perspective resulting bearing capacities from the two extrema is shown in table 2.5. For this specific set of parameters there is an increase in bearing capacity of more than 30% from the more conservative solution.

Table 2.5: Bearing capacities for $A' = 1\,m^2$, $c' = 0\,{}^{kN}/_{m^2}$, $q' = 0\,{}^{kN}/_{m^2}$ and $\gamma' = 20\,{}^{kN}/_{m^3}$.

Equation 2.38	$\varphi = 30^o$	$\varphi = 35^o$	$\varphi = 40^o$
Eurocode 7	60 kN	136 kN	318 kN
DNV no. 30.4	45 kN	102 kN	239 kN

As mentioned in section 2.1.1 the cohesion is often set to zero for frictional soils in danish geotechnical practice. For soils which fall somewhere in between perfectly cohesive and frictional, this choice may come at a rather large expense or on the other hand possibly fatal consequences. Table 2.6 shows a fictitious example of this.

Table 2.6: Influence of cohesion on bearing capacity for $A' = 1m^2$, $q' = 0{}^{kN}/_{m^2}$ and $\gamma' = 20{}^{kN}/_{m^3}$.

Equation 2.38	$\varphi = 30^o$	$\varphi = 35^o$	$\varphi = 40^o$
$c = 2\ {}^{kN}/_{m^2}$	116 kN	213 kN	433 kN
$c = 0\ {}^{kN}/_{m^2}$	44 kN	102 kN	253 kN

This simple example reveals the hazards of using a spurious cohesion or the loss by not using a cohesion which is actually accountable, depending on the viewpoint.

Specifically in the context of this study, circular footings are of great interest. Such structures are usually approximated as an equivalent square, when using bearing capacity formulae. Studies have shown that for square and circular footings of equivalent area, the square have a larger bearing capacity [22]. This intuitively discredits the assumption for circular footings. It can though still be justifiable if used with the shape factor, s_γ, proposed by Brinch-Hansen (1970). This should lead to conservative results in both cases, as will be discussed further in chapter 5.

2.3.3 Non-linear Finite Element Method

Solving geotechnical boundary value problems with a traditional linear finite element method is rarely sufficient. The method has though been adapted to cope with non-linearities of the constitutive models used for soils. Several procedures accommodate this need. Common for them all is that either load or displacement boundary conditions are applied incrementally and equilibrium is sought iteratively. Finite element analyses in this thesis are conducted in PLAXIS. For the standard Mohr-Coulomb model implemented in the software a linear stiffness iteration method is used. In user defined models it is possible to use either a linear stiffness, full Newton-Raphson or modified Newton-Raphson iterative method. For the purposes of this study the standard procedures in PLAXIS is utilized and user defined models will be programmed coherently. An advantage of the linear stiffness iterative method is that it operates with the elastic stiffness matrix for all steps in the calculation procedure. This implies that the stiffness matrix only needs to be formed and decomposed at the first calculation step [23]. Linear stiffness iterative procedures are illustrated in figure 2.19. A disadvantage to this procedure is that it generally requires more iterations, than its counterparts, to reach a solution point. This becomes obvious by comparing to the full Newton-Raphson where a tanget stiffness matrix is formed at every iteration.

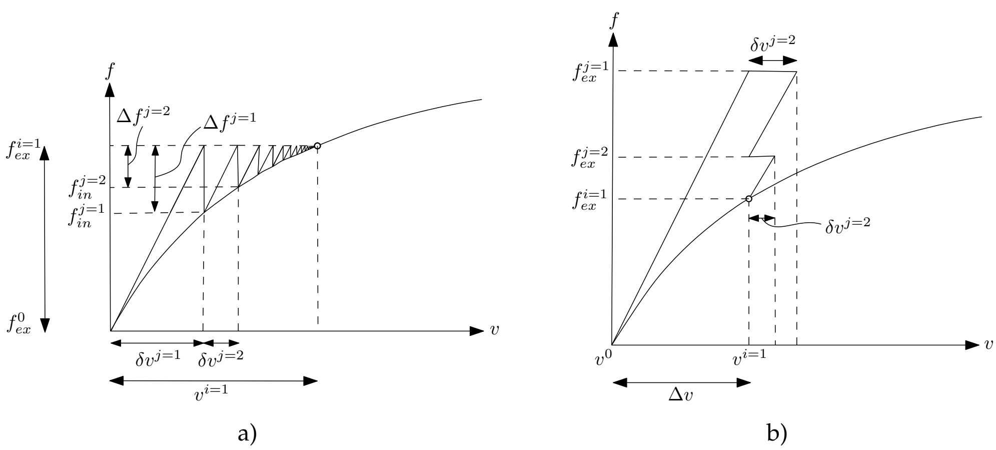

Figure 2.19: Iterative process illustrated for a) Prescribed force b) Prescribed displacement.

The overall idea is to approximate the non-linear behaviour with piecewise linear segments between solution points which are determined iteratively. The key steps for solving this is explained for a load controlled incremental procedure in this section. From a specified load increment a displacement increment is determined as

$$\Delta \boldsymbol{v} = \boldsymbol{K}^{-1} \Delta \boldsymbol{f} \tag{2.40}$$

From this displacement a strain increment is computed through the strain interpolation matrix

$$\Delta \boldsymbol{\varepsilon} = \boldsymbol{B} \Delta \boldsymbol{v} \tag{2.41}$$

From this increment the constitutive stresses are calculated as in section 2.2 and the resisting force in the system can be determined.

$$\boldsymbol{f}_{in} = \int_V \boldsymbol{B}^T \boldsymbol{\sigma} dV \tag{2.42}$$

The external force is the sum of the previous and current increments. A residual is determined as the difference between the external force and the resisting force.

$$\Delta \boldsymbol{f}_{res} = \boldsymbol{f}_{ex} - \boldsymbol{f}_{in} \tag{2.43}$$

This residual force is then used to determine a displacement adjusting the one from the present iteration

$$\delta \boldsymbol{v} = \boldsymbol{K}^{-1} \Delta \boldsymbol{f}_{res} \tag{2.44}$$

which is added to the initial displacement increment. This procedure is repeated until the residual force reaches a user specified margin of error. The full calculation process for load controlled and displacement controlled analysis is outlined schematically in the following flowcharts.

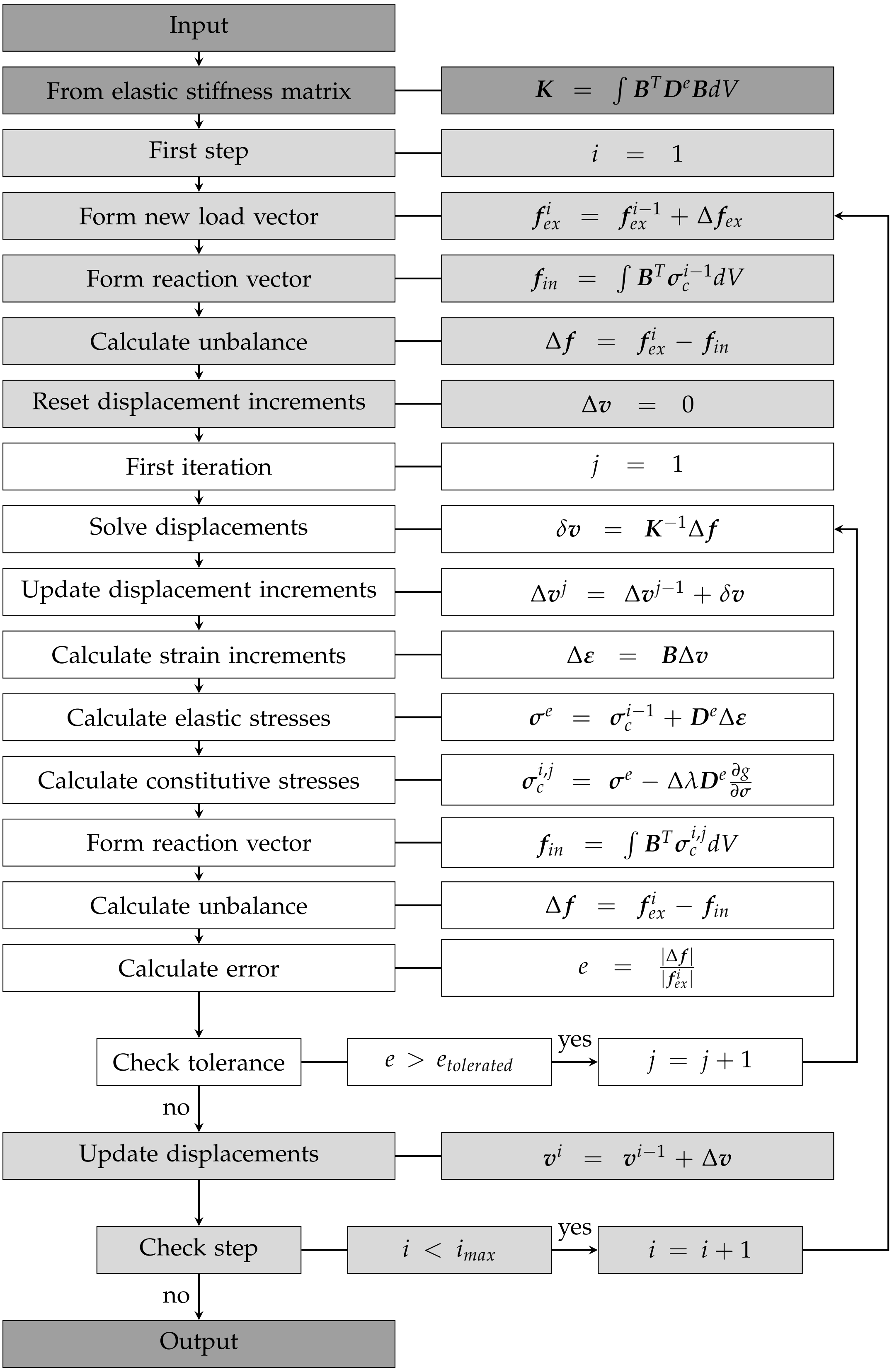

Figure 2.20: Finite element calculation process based on the elastic stiffness matrix with load control [23]

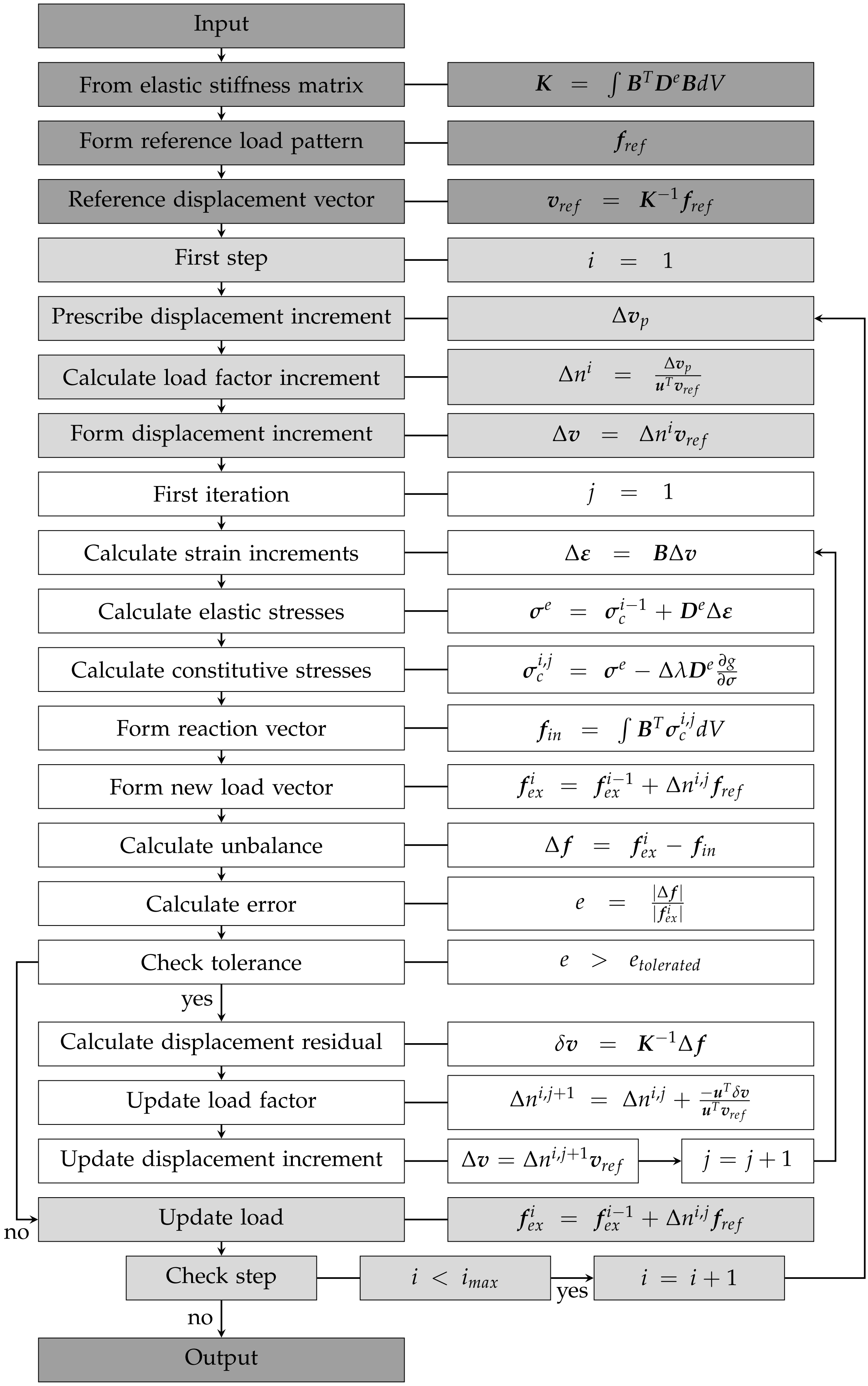

Figure 2.21: Finite element calculation process based on the elastic stiffness matrix with displacement control [24]. $\boldsymbol{u}$ is a vector containing all zeros, except for ones at prescribed displacements.

Chapter 3

The General Parametric Yield Surface Format

This chapter provides a brief introduction to a general parametric yield surface format, proposed by Lars Damkilde. The yield criteria is proposed in three versions of increasing complexity and hereby also capabilities of representing material behaviour. The models are not described in their entirety in this thesis, which rather focuses on some select key features and how these deviate from the constitutive models most frequently used by practitioners today. A more thorough mathematical description is presented in [25]. The general parametric yield surface is able to emulate a large variety of acknowledged yield criteria, but for the purposes of this thesis the Mohr-Coulomb criterion will serve as a benchmark. The variability is illustrated in figure 3.1.

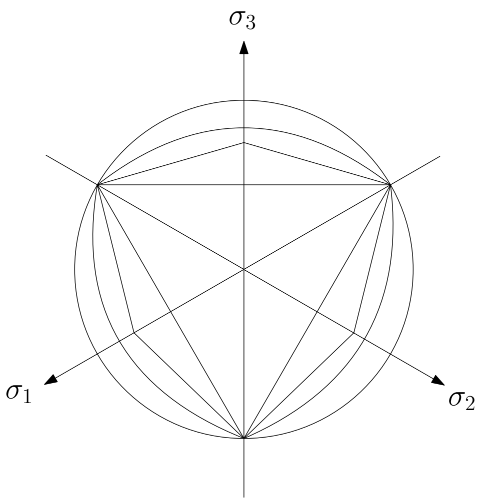

Figure 3.1: Deviatoric variability of the general parametric yield surface format.

3.1 Fundamental Principles for Formulation

The yield surface is conveniently formulated from a coordinate system in which one axis coincide with the hydrostatic axis and the two other axis lie in the π-plane.

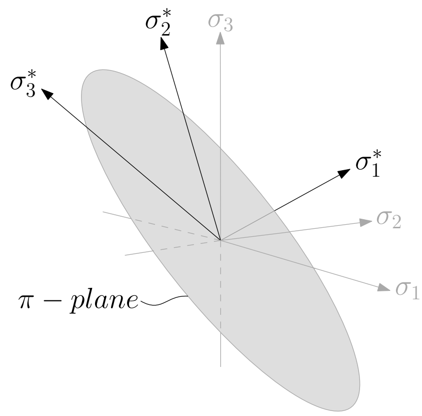

Figure 3.2: Rotation of coordinate system.

The transformation to this coordinate system from principal stresses is given by

$$\begin{Bmatrix} \sigma_1^* \\ \sigma_2^* \\ \sigma_3^* \end{Bmatrix} = \begin{bmatrix} 1/\sqrt{3} & 1/\sqrt{3} & 1/\sqrt{3} \\ -\sqrt{2/3} & 1/\sqrt{6} & 1/\sqrt{6} \\ 0 & -1/\sqrt{2} & 1/\sqrt{2} \end{bmatrix} \begin{Bmatrix} \sigma_1 \\ \sigma_2 \\ \sigma_3 \end{Bmatrix} \tag{3.1}$$

By inspecting this it is clear to see that the hydrostatic stress can be found from σ_1^* and the deviator stress from σ_2^* and σ_3^* as

$$p = \frac{\sigma_1^*}{\sqrt{3}} \quad \wedge \quad \rho = \sqrt{(\sigma_2^*)^2 + (\sigma_3^*)^2} \tag{3.2}$$

through simple geometric relations. In its simplest form the criteria is defined from a center and radius based on strength parameters for the material to be modelled. This can be visualized as tracing a circle in the deviatoric plane, where the criteria holds true for the part of the circle enclosed by the deviatoric region for which the chosen ordering of principal stress applies. Like the Mohr-Coulomb yield criterion there is sixfold symmetry which can be exploited to formulate the criterion for all arrangements of principal stresses.

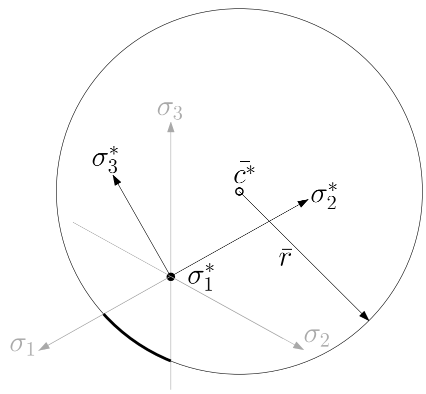

Figure 3.3: Principle sketch forming the deviatoric geometry of the yield surface. $\overline{c^*}$ and $\bar{r}$ represent ρ_c-normalized center and radius.

One of the absolute essential features of the novel yield surface, compared to the Mohr-Coulomb criterion, is the ability to include effects stemming from variation of the intermediate principle stress. This is done by introducing parameters α and β, which controls the ρ_t/ρ_c-ratio and the side curvature respectively. This is illustrated in figure 3.4. Essentially the parameters control where the center is placed and the magnitude of the radius. The specific formulations relating α and β to the center and radius will not be reviewed in this thesis, but are included in the source code for the PLAXIS implementation of the yield criteria.

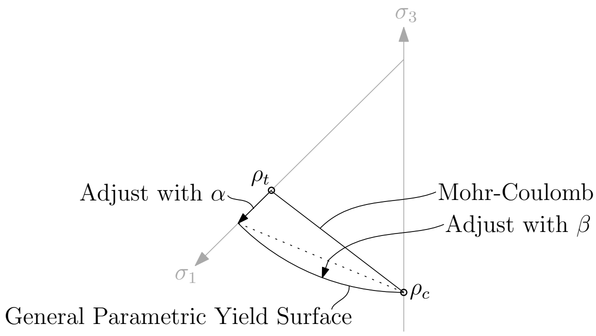

Figure 3.4: Visual representation of the implications from adjusting α and β.

The simplest form of the general parametric yield surface result in a discontinuous deviatoric trace, which can be an issue in numerical solutions. This is obviously not true if the parameters are set so that the criteria emulates Drucker-Prager. The apex in the meridian plane pose the same issue, regardless of the shape in the deviatoric plane. To avoid non-unique gradients at the discontinuities, the yield criteria can be extended to include a corner rounding in the deviatoric plane and apex rounding in the meridian plane.

This thesis only perform analysis using the general parametric yield surface with a linear trace in the meridian plane. The compressive meridional eccentricity is defined as in the traditional Mohr-Coulomb yield criterion. From this ρ_c can be expressed as a function of the hydrostatic pressure

$$\rho_c = \mu \left(p - \frac{\sigma_c}{k-1} \right) \quad \wedge \quad \mu = \frac{1-k}{\sqrt{2/3}(k/2+1)} \tag{3.3}$$

where σ_c and k are as in the Mohr-Coulomb criterion and μ is the slope of the yield criteria in the compressive meridian plane. The resulting ρ_c is then used to scale the yield function according to the relevant stress level. In this manner the well-known parameters for cohesion and friction angle is used to formulate the meridional variation.

3.2 Overview of Versions

The three different versions of the proposed yield functions are all formulated in the same format with some underlying differences. The straight line distance between the center and the stress point is determined and the radius is subtracted. As such a negative value of the yield function represent an elastic state, as per usual. Common for all formulations, only the deviatoric components of the $\boldsymbol{\sigma}^*$ are stated directly in the yield function.

$$\boldsymbol{\sigma}_d^* = \begin{Bmatrix} \sigma_2^* \\ \sigma_3^* \end{Bmatrix} \tag{3.4}$$

The σ_1^* component is indirectly represented in ρ_c which scales the function to the proper hydrostatic stress level.

The 4 parameter General Parametric Yield Surface has linear variation on hydrostatic pressure and a discontinuous deviatoric trace. The parameters are as introduced in the fundamental formulation of the yield criteria. Namely φ, c, α and β.

$$f(\sigma) = \|\boldsymbol{\sigma_d^*} - \overline{\boldsymbol{c_1^*}}\rho_c\| - \overline{r_1}\rho_c \tag{3.5}$$

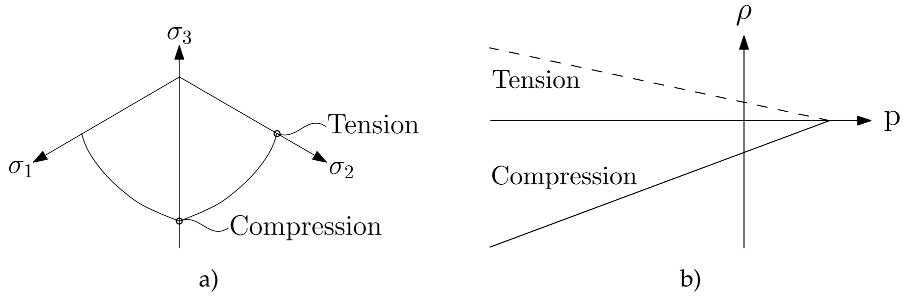

Figure 3.5: a) Deviatoric trace, b) Meridional plane.

The 7 parameter General Parametric Yield Surface has linear variation on hydrostatic pressure and a continuous deviatoric trace. The version introduces corner and apex roundings to improve performance in numerical analysis. This is done by introducing parameters β_2, β_3 and β_4 controlling roundings at the two deviatoric corners and meridional apex respectively. The yield function now operates with three regions per sixth of the full deviatoric trace. The apex rounding is inherent in the determination of ρ_c.

$$f_n(\sigma) = \|\boldsymbol{\sigma_d^*} - \overline{\boldsymbol{c_n^*}}\rho_c\| - \overline{r_n}\rho_c \tag{3.6}$$

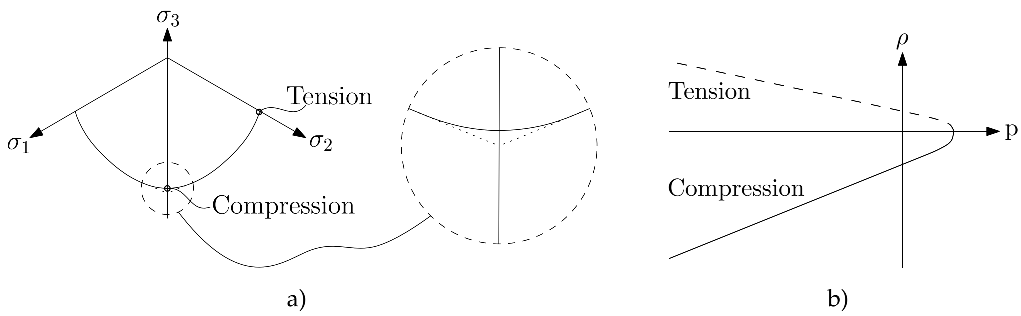

Figure 3.6: a) Deviatoric trace, b) Meridional plane.

The 10 parameter General Parametric Yield Surface with non-linear variation on hydrostatic pressure and continuous deviatoric trace. Although not used in analysis for this thesis, this criteria is briefly presented to illustrate the capabilities of the format. The meridional non-linearity can in principle be formulated from any appropriate function, which may alter the number of parameters required. The version with 10 parameters is formed from the Bolton criterion and can be explored further in [25].

$$f_n(\sigma) = \|\boldsymbol{\sigma}_{\boldsymbol{d}}^* - \boldsymbol{c}_{\boldsymbol{n}}^*(p)\| - r_n(p) \tag{3.7}$$

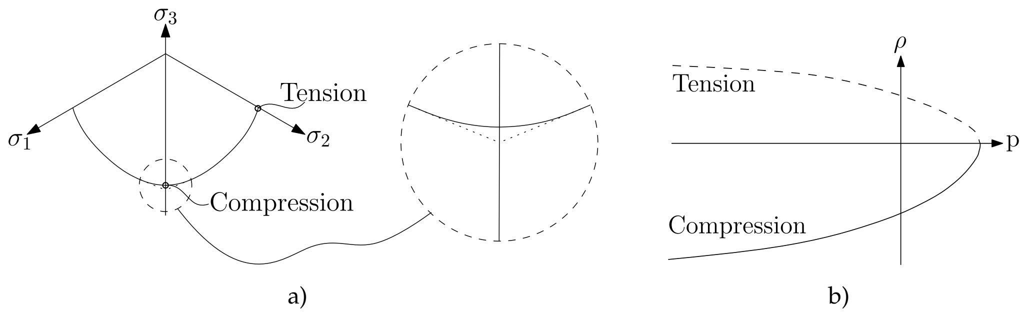

Figure 3.7: a) Deviatoric trace, b) Meridional plane.

3.3 Unconventional Soil Testing

To utilize the capabilities of the proposed General Parametric Yield Surface, it is necessary to revise the soil tests to be conducted within a given project. The fact that a variation of the intermediate principal stress does influence the behaviour of a soil volume, becomes very apparent in true triaxial test results, as depicted in figure 3.8.

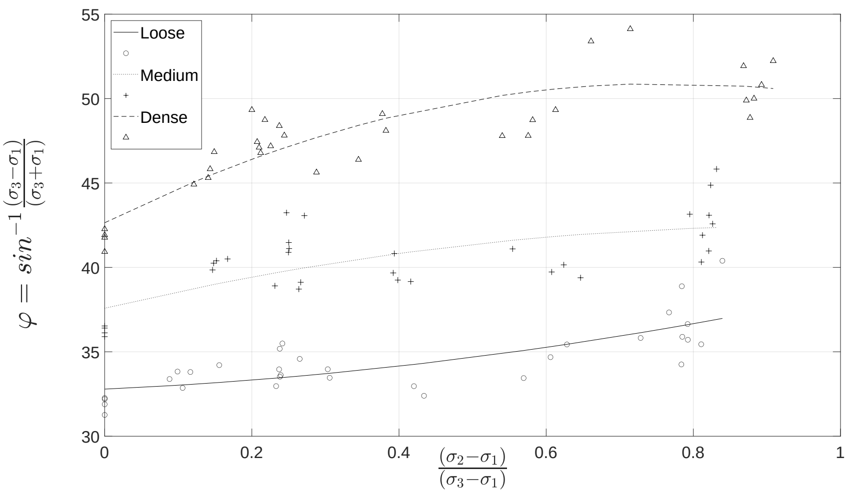

Figure 3.8: Development of friction angle from triaxial compression approaching triaxal extension.

The Mohr-Coulomb yield criterion operates with a fixed ρ_t/ρ_c relation. The validity and possible correction of this can be evaluated by conducting triaxial extension test. Many studies has shown, that ρ_t is underestimated, indicating that a larger elastic domain can be modelled if extension tests are implemented as a fundamental test in soil mechanics. Thus, as an alternative to conventinal compressive triaxial test, this thesis proposes true triaxial tests and triaxial extension tests to find more accurate strength parameters.

Extension Soil Testing It is not possible to extend soil by pulling, hence an extension test can not be conducted reverse to the compression triaxial test. An extension triaxial test is made with pressure on the sides of the specimen allowing axial displacements. The soil test is loaded in the horizontal direction with the largest compressive principal stress as depicted in figure 3.9. Opposed to the compressive triaxial test, the intermediate principal stress will coincide with the largest compressive stress.

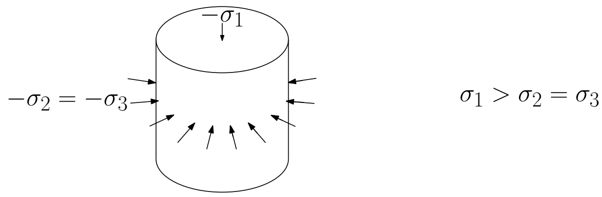

Figure 3.9: Extension triaxial test.

True Triaxial Soil Testing The conventional triaxial test uses only the largest and smallest stress to find strength parameters, which is a very conservative approach as the assumption of $-\sigma_1 = -\sigma_2$ is the stress combination, that gives the absolute smallest triaxial friction angle. In attempt to simulate more realistic strength parameters, the relation between the friction angle and the intermediate principle stress is investigated by the true triaxial test, which is described in this section. For a more thorough description of the true triaxial test see [5]. It is important to mention that there are a number of different apparatus for these test with slight differences. The overall principle is though the same.

The principle of the true triaxial test is that stresses can be controlled in three different directions and so samples are typically are cubical or rectangular prisms. This allows for exact control of the magnitude of the intermediate principle stress, in relation to the major and minor principal stress. There are pressure heads on two opposing horizontal sides and one at the top. The bottom plate is fixed. The minor principal stress is controlled by a vacuum in the sample. The principle of the true triaxial test is depicted in figure 3.10.

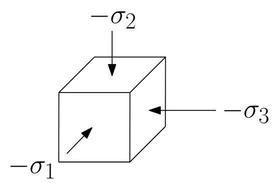

Figure 3.10: True triaxial test.

The stiff and smooth pressure heads are applied as in the conventional triaxial test. The volumetric strains can be calculated by measuring the axial strain in all three directions in the usual way and found from equation 3.8.

$$\varepsilon_V = \varepsilon_1 + \varepsilon_2 + \varepsilon_3 \tag{3.8}$$

By testing at different intermediate stress levels, it is possible to approximate a better yield surface.

Chapter 4

Modelling

This chapter goes through how the specific material models in present report are calibrated and utilized in numerical analysis. Besides this, some general considerations for geotechnical problems solved in a elasto-plastic finite element framework are presented. Some represent specific considerations related to determination of the ultimate bearing capacity for footings. Others are more general for finite element analysis. As in all aspects of engineering it is important to be aware of what output and accuracy you expect from your models.

4.1 General Considerations

The initial stresses in a soil domain are generated through the K_0 procedure in PLAXIS. This is simply relating the vertical and horizontal stresses through the relation

$$\sigma'_{xx} = \sigma'_{yy} = \sigma'_{zz} K_0 = (\gamma' d + p) K_0 \tag{4.1}$$

Here, stated for a three dimensional case. K_0 is the at rest soil pressure coefficient approximated as in equation 4.2. γ is the specific weight, d is the depth and p represents any potential surface pressure.

$$K_0 = 1 - sin(\phi') \tag{4.2}$$

The procedure is suitable for the analysis performed in present thesis, but alternatives must be used when dealing with e.g. sloping surfaces or soil layers with a geological history affecting the lateral soil pressure.

The stiffness of the structure affects how the stresses are distributed [3] in the soil volume. This is conveniently illustrated under the assumption of linear-elastic, isotropic and homogeneous soil, in figure 4.1. Two extrema are represented by a rigid structure and a flexible structure. The former will theoretically produce infinitely large stresses at the edge of the structure and a uniform settlement profile. The latter produces a uniform stress distribution under the entire footing and a concave settlement profile, see figure 4.1.

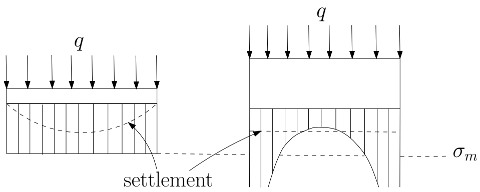

Figure 4.1: a) Elastic footing. b) Rigid footing.

The analysis performed in chapter 5 are all conducted with a prescribed surface or line displacement, simulating a rigid footing.

The soil-structure interface varies from rough to smooth, and the two extrema are described in present section. In attempt to simulate the soil-structure interaction of the two extrema in PLAXIS the aforementioned displacement is applied in a plane strain analysis of a strip footing. The displacement of the structure is constrained horizontally to emulate a completely rough interface and is released to create a completely smooth interface. The corresponding failure modes a depicted in figure 4.2.

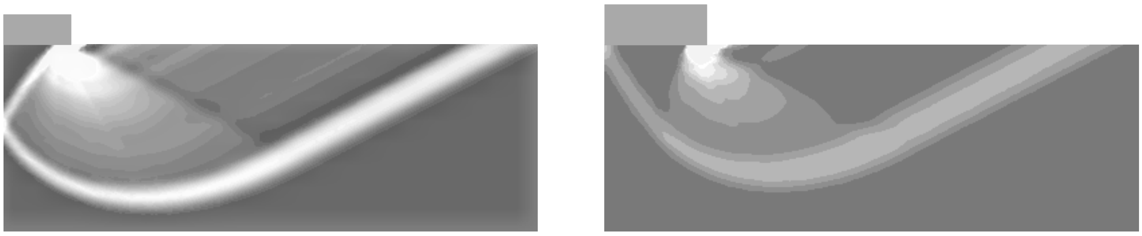

a) b)

Figure 4.2: a) Failure mode rough interface b) Failure mode smooth interface

As a result of the failure mechanisms, the smooth solution will result in a lower load at failure, as less soil, opposite the rough solution, move towards the outer edge and the surface, when the strip footing is loaded.

In general the soil will not behave as neither fully smooth or rough, hence a specific interface strength between 0 and 1 can be specified in PLAXIS by prescribing a specific strength reduction factor, which gives a more realistic suggestion on the strength of the interface. The reduction factor relates the friction angle of the soil volume and the friction angle in the interface as

$$R_{int} = \frac{tan(\delta)}{tan(\varphi)} \tag{4.3}$$

Where δ is the interface friction angle. This is often troublesome to quantify and a complete study in its own. When a user defined material model is utilized the interface must be defined explicitly through a set of strength parameters for the interface, e.g. the friction angle and cohesion.

The domain size in geotechnical finite element models have a sufficient extent to represent the relevant behaviour of the soil. The stress field must be able to develop to an extent where variations are no longer of any practical influence [26]. Some guidelines for deciding a proper domain size do exist, but it is troublesome to generalize such, as it is essentially a problem specific matter. To facilitate better decision-making a minor investigation of the influence of domain size is performed. The necessary depth of the domain depends on what the designer wants out of an analysis. An accurate displacement response requires a relatively deep domain, which intuitively makes sense as noticeable settlements will occur to a considerable depth. This is demonstrated through a depth variation of the soil domain for a strip footing in plane strain analysis.

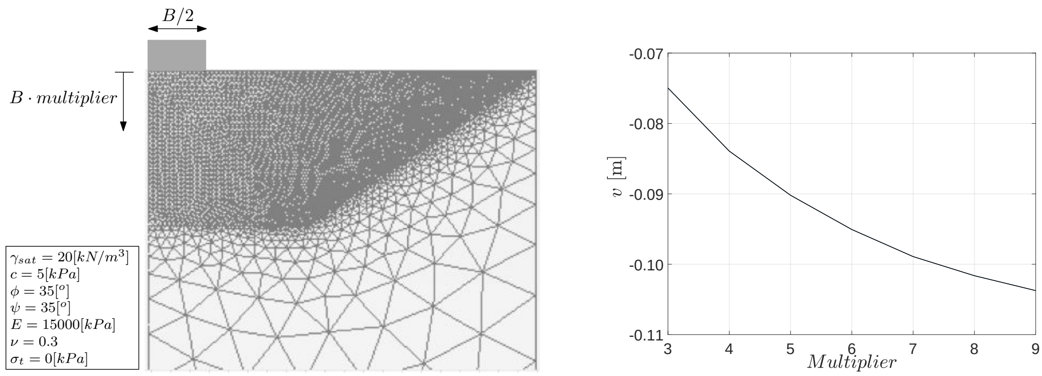

a) b)

Figure 4.3: Displacements with depth variation.

There is no convergence as such, as minor settlements will accumulate, even at great depths. The rate of the increase does though decrease and the credibility of the results could be enhanced by incorporating a stiffness increase with depth. The ultimate load bearing capacity is nearly constant for all the depths represented.

Care must be taken so the analysis do not suffer boundary effects leading to e.g. unrealistic failure modes. For the structures under investigation the depth of the soil domain needed for the stress field, is by far sufficient for the failure mechanism. The horizontal extend of the domain must though be carefully chosen based on the applied strength parameters and yield criterion. This is illustrated in figure 4.4.

a) b)

Figure 4.4: a) Correct failure mode b) False failure mode

Choosing a very large domain compared to the structure will undoubtedly bypass all the issues addressed. This will though be costly in computational time, without any substantial benefit towards the accuracy of the solution. The designer should aim at a compromise which suits the problem at hand.

Meshing is, as in all finite element analysis, a key aspect in obtaining acceptable approximations of a geotechnical problem. The mesh must be sufficiently fine to obtain a solution of the desired accuracy. On the other hand, calculation time is preferably kept at a minimum. PLAXIS does not offer the most sophisticated options for mesh generation. The global elements are sized from a factor multiplied onto the diagonal of the soil domain. Any desired local refinements are then generated for a selected area or volume by a factor multiplied onto the global element size. These refinements range between 1/32 to 8 in PLAXIS 2D and between 1/16 to 8 in PLAXIS 3D, where values above 1 obviously coarsens the mesh. This procedure may cause a unwanted fineness of the global element in order to obtain a desired local fineness, which ultimately affects the calculation time. This is illustrated through a numerical example with of a strip footing in plane strain analysis.

Table 4.1: Convergence of mesh refinement. Global mesh value 0.2, except for the finest mesh.

Refinement	1/2	1/4	1/8	1/16	1/24	1/32	(1/43)
Elements	113	270	773	2516	5352	9015	15922
Nodes	963	2237	6307	20333	43105	72487	127865
Calc. time [s]	32	41	110	414	891	1742	3121

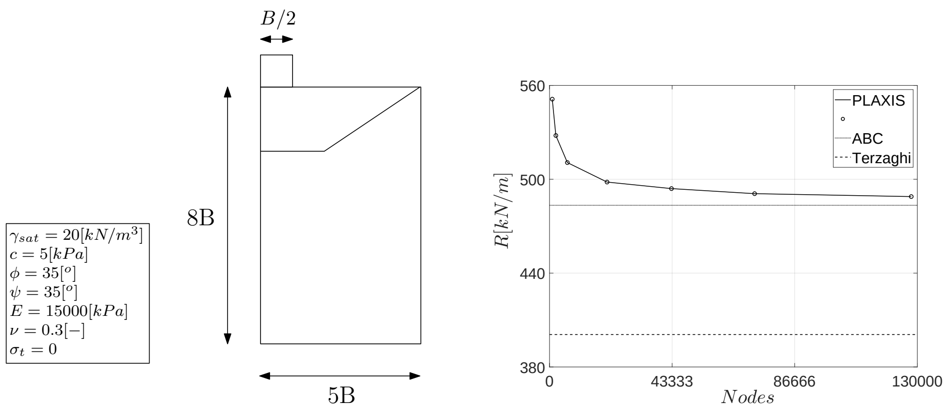

a) b)

Figure 4.5: a) Finite element model b) Convergence of bearing capacity

The solution does converge to an extend suitable for most analysis within the given framework of the refinement. If more accuracy is required it is necessary to refine the mesh globally to obtain the desired element size locally. This undoubtedly requires more elements, than if the local refinements could be performed more freely, as illustrated in figure 4.5.

4.2 User Defined Material Model in PLAXIS

In PLAXIS it is possible to create a user defined soil model. This model is programmed in Fortran language and compiled as a dynamic link library, which is then added to the

"UDSM" sub-folder of the PLAXIS program directory. This section is intended to provide a brief overview for the generation of a user defined soil model subroutine for PLAXIS. For a thorough description of the structure and options for subroutines see [PLAXIS MANUAL MATERIAL MODELS]. Furthermore the specific choices made for the particular model programmed for this thesis are presented. The subroutine is written in fixed form fortran with implicit double precision merely to stay consistent with models provided by PLAXIS. The structure of the subroutine is:

Subroutine User_Mod *(IDtask, iMod, IsUndr, iStep, iTer, Iel, Int, X, Y, Z, Time0, dTime, Props, Sig0, Swp0, StVar0, dEps, D, Bulk_W, Sig, Swp, StVar, ipl, nStat, NonSym, iStrsDep, iTimeDep, iTang, iPrjDir, iPrjLen, iAbort)*

Some of the parameters stated are provided by PLAXIS as input to the subroutine, while others are intended as an output from the subroutine. An overview is presented in table 4.2.

Table 4.2: Parameters in subroutine. Inputs are provided by PLAXIS and outputs are provided by the user. The values listed are specific to the model programmed in present thesis.

Name	Description	I/O	Type	Value
IDtask	Task called by PLAXIS	I	Integer	1:6
iMod	Selection of model	I	Integer	1
IsUndr	Drained or undrained	I	Integer	0:1
iStep	Calculation step	I	Integer	-
iter	Iteration number	I	Integer	-
Iel	Element number	I	Integer	-
Int	Local stress point	I	Integer	-
X, Y, Z	Global coordinates for stress point	I	Real	-
Time0	Time	I	Real	-
dTime	Time increment	I	Real	-
Props	Model parameters	I	Integer	1:10
Sig0	Stress and variables	I	Real	-
Swp0	Excess pore pressure	I	Real	-
StVar0	State variables	I	Real	-
dEps	Strain increment	I	Real	-
iPrjDir	Project directory	I	Characters	-
iPrjLen	Length of directory name	I	Integer	-
D	Material stiffness matrix	O	Real	-
Bulk_W	Bulk modulus of water	O	Real	-
Sig	Constitutive stress	O	Real	-
Swp	Excess pore pressure	O	Real	-
StVar	State variables	O	Real	-
ipl	Plasticity indicator	O	Integer	0:2
nStat	Number of state variables	O	Integer	0
NonSym	Non-symmetric D-matrix	O	Integer	0
iStrsDep	Stress dependent D-matrix	O	Integer	0
iTimeDep	Time dependent D-matrix	O	Integer	0
iTang	Tangent D-matrix	O	Integer	0
iAbort	Force calculation to stop	O	Integer	1

There are essentially six tasks that a user defined soil model programmed for PLAXIS must be capable of solving, see table 4.3. These tasks are called from the subroutine via the integer input from PLAXIS, named IDtask.

Table 4.3: Tasks in user defined soil model in the sequence called by PLAXIS.

IDtask	Intended task
4	Return the number of state variables
5	Return matrix attributes
1	Initialize state variables
3	Create effective material stiffness matrix
2	Calculate the constitutive stresses
6	Create elastic material stiffness matrix

As a linear stiffness iteration method is chosen, much like the standard PLAXIS models, tasks 3 and 6 will coincide. More generally task 6 is used to determine a relative stiffness parameter relating the actual stress state to that of a fully elastic body, given by equation 4.4. This is used as a control parameter, which approaches zero at failure, in determination of the global error of the solution.

$$CSP = \int \frac{\Delta\varepsilon\Delta\sigma}{\Delta\varepsilon D'\Delta\varepsilon} \tag{4.4}$$

No state variables are used in the general parametric yield surface model written. This means that task 4, 5, 1, 3 and 6 are only called in the beginning of each calculation phase, so that each step basically have the same offset. Task 2 is called at every iteration. This is also the only task, which for the model programmed in this thesis, must be treated meticulously, as the other tasks are rather trivial. For the purposes of this thesis it is chosen to implement the general parametric yield surface in its simplest form. Besides the principles outlined in chapter 3 a simple tension cut off is introduced. In essence it functions much like the apex rounding, merely without the smooth approximation. A parameter β_t can be chosen between 0 and 1 where the former allows no positive hydrostatic stress states and the latter indicates no tension cut off.

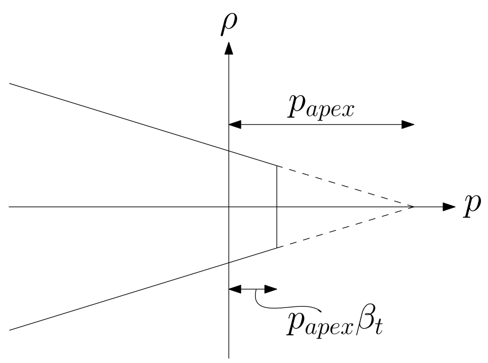

Figure 4.6: Simple tension cut off procedure in user defined soil model.

4.3 Calibration of Material Models

As mentioned in section 2.2.1 the standard Mohr-Coulomb model in PLAXIS is composed of a elastic law, a yield criterion and a flow rule. The same applies to the user defined model programmed, which will be referred to as the General Parametric model. The difference lie in the yield criteria and consequently also the flow rule. The calibration of elastic parameters are identical for both models. The parameters to be calibrated for the Mohr-Coulomb model is as stated in table 2.3. Data from compressive triaxial tests performed on baskarp sand no. 15 is used to illustrate calibration of elastic parameters and the more conventional fitting methods for the Mohr-Coulomb yield criteria. Data from true triaxial tests on G-12 sand is used to calibrate both the Mohr-Coulomb model and the General Parametric model, to be used in comparative analyses.

The secant modulus is found at 50% of the deviatoric stress at failure as illustrated in figure 4.7. From this point the secant modulus is found from Hooke's law by $E_{50} = \rho_{50}/\varepsilon_{50}$.

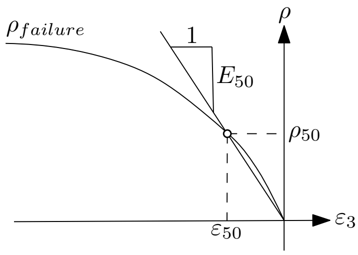

Figure 4.7: Secant modulus

Depth variation of stiffness can be modelled to increase the accuracy of the load-displacement response. In PLAXIS this can be done by specifying young's modulus at a reference level and linearly increasing this with depth.

$$\begin{aligned} E'(y) &= E'_{ref} + (y_{ref} - y)E'_{inc} \qquad for \quad y < y_{ref} \\ E'(y) &= E'_{ref} \qquad\qquad\qquad\qquad for \quad y > y_{ref} \end{aligned} \tag{4.5}$$

In practice this linear approximation can be fitted to the elastic moduli obtained at various confining pressures from triaxial tests. The depth equivalent to the confining pressure is obtained from the at rest earth pressure

$$y = -\frac{\sigma_1'}{\gamma' K_0} \quad where \quad K_0 = 1 - sin(\varphi') \tag{4.6}$$

Test results indicate that the stiffness varies non-linear and so the linearisation inevitably under- or overestimates the stiffness through the soil volume. The specific moduli used for analysis in this thesis are extrapolated so that the reference level is at the footing level.

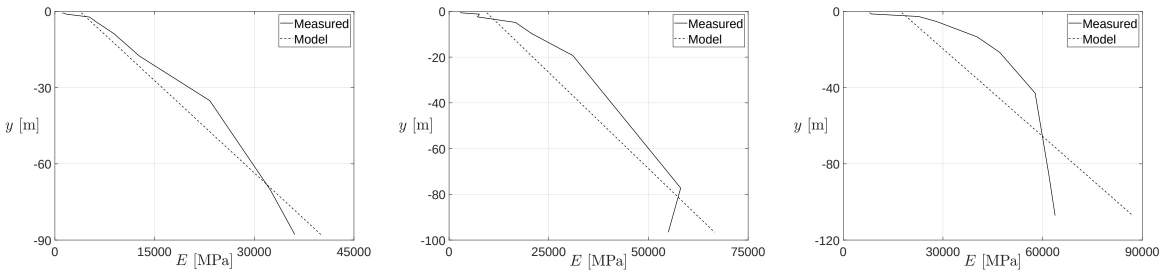

a) b) c)

Figure 4.8: Depth dependent stiffness for a) loose b) medium c) dense.

The dilatancy angle is determined from a compressive triaxial test as the maximum rate of volumetric strain relative to the axial strain. The angle ψ is determined as in equation 2.8. This is done under the assumption that the elastic strains are negligible compared to the plastic strains. The results from baskarp sand no. 15 is shown for loose, medium and dense deposits in figure 4.9.

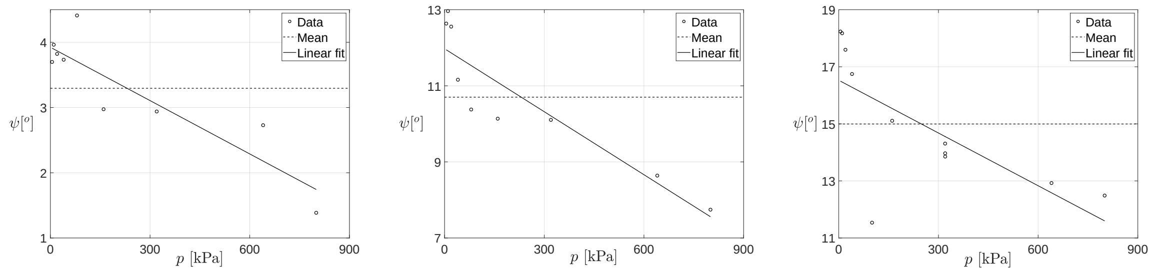

a) b) c)

Figure 4.9: Dilatancy angle illustrated for a) loose b) medium c) dense.

There is a clear tendency for the dilatancy angle to decrease with confining pressure. For the analysis to be performed in this thesis the mean dilatancy angle will be utilized. These all lie well above the often used simple relation from equation 2.7, as shown in table 4.5.

Table 4.4: Comparison of dilatancy angles for baskarp sand no. 15.

		Loose	**Medium**	**Dense**
$\psi = \varphi' - 30$	$[^o]$	1.13	5.32	9.02
$\overline{\psi}$	$[^o]$	3.30	10.70	14.99

Observations from true triaxial tests do not show the tendency of decreasing dilatancy angle with confining pressure, or more fittingly in this case hydrostatic pressure. A least squares fit nearly coincide with the mean angle of all tests, see figure 4.10. Although not substantial to disprove the broadly accepted decrease in dilatancy angle with increasing confining pressure, it supports the use of a mean angle for the purposes of this study.

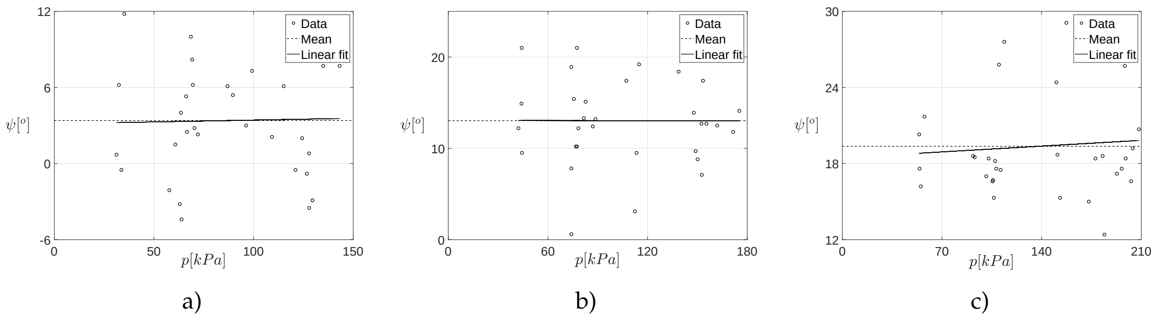

Figure 4.10: Dilatancy angle from true triaxial test for a) loose b) medium c) dense.

As for the results obtained from the more conventional triaxial test, the data evidently substantiate the conservatism of equation 2.7. This holds true for both the compressive triaxial equivalent results and the entire dataset, which also contains values approaching an extensive triaxial state.

Table 4.5: Comparison of dilatancy angles for G-12 sand.

		Loose	**Medium**	**Dense**
$\psi = \varphi' - 30$	$[^o]$	1.50	6.22	10.67
$\overline{\psi}$	$[^o]$	3.39	13.03	19.36

4.3.1 The Mohr-Coulomb Model

As shown in section 2.2.1 a failure line can be fitted as the best possible tangent to Mohr's circles in a σ-τ diagram. This is likely to become incomprehensible as the amount of tests to be fitted increases. On the other hand more tests and hence more data will undoubtedly increase the credibility of the model. To generate the Mohr-Coulomb criterion from larger datasets it is common practice to present stresses at failure in points rather than Mohr's circles. The principle is illustrated in figure 4.11

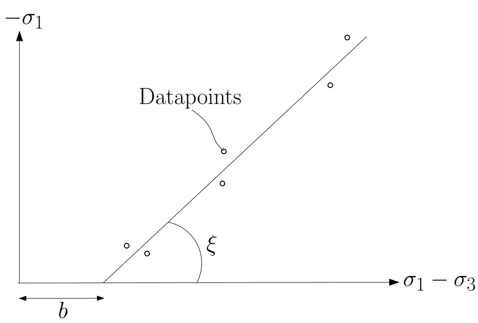

Figure 4.11: Conventional fitting procedure of the Mohr-Coulomb yield surface.

The confining pressure is plotted against the deviatoric stress. The procedure is performed on baskarp sand no. 15, as seen in figure 4.12.

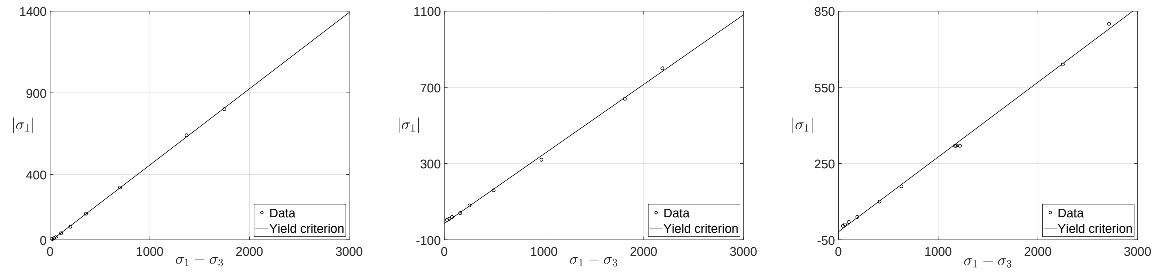

a) b) c)

Figure 4.12: Conventional fitting procedure of Mohr-Coulomb for a) loose b) medium c) dense.

By linear least squares regression a line is fitted to the data points. The friction angle and cohesion can then be determined through the relations in equation 4.7 [3] and the resulting parameters are shown in table 5.3.

$$\varphi' = sin^{-1}\left(\frac{1}{1+2tan(\xi)}\right) \quad \wedge \quad c' = btan(\xi)tan(\varphi') \tag{4.7}$$

Table 4.6: Strength parameters for baskarp sand no. 15

		Loose	**Medium**	**Dense**
φ'	$[^o]$	31.13	35.32	39.02
c'	[kPa]	5.27	10.00	14.49

The fittingness of the procedure is illustrated with residual plots in figure 4.13 and corresponding statistics in table 4.7.

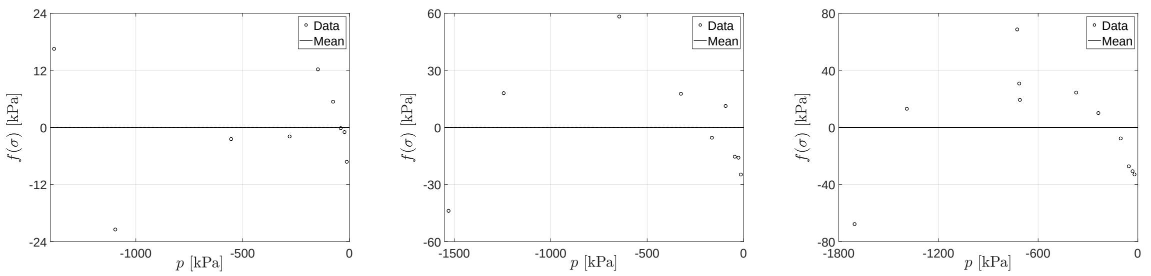

a) b) c)

Figure 4.13: Residual plots.

Table 4.7: Evaluation of calibrations. All values in [kPa].

Baskarp sand no. 15	Loose	Medium	Dense
$\overline{f(\sigma)} = \frac{1}{N}\sum_{i=1}^{N} f(\sigma_i)$	0.0001	0.0017	0.0011
$\sigma = \sqrt{\frac{1}{N}\sum_{i=1}^{N}(f(\sigma_i) - \overline{f(\sigma)})^2}$	11.04	30.03	37.84
$max(\lvert f(\sigma_i)\rvert)$	21.46	58.30	68.69

The deviations show a clear weakness of the linearisation involved in the fitting. The error becomes more renounced by increase in both the density index and confining pressure. At a first glance the numeric deviations from the yield criterion seem vast. It must be noted though that some of the tests involved are performed at relatively high stress levels. By simulating a triaxial test with the Mohr-Coulomb model in PLAXIS the discrepancy between the measured results and the model become very apparent, as seen in figure 4.16.

Generally the deviations are reasonable, in ultimate limit state context, but at the lower stress levels the deviator stress is significantly higher for the model. This most likely occurs as the cohesion is determined from a linear fit to all data points, which will overestimate the cohesion at lower stress levels. From compressive triaxial test simulations performed with and without cohesion for all other parameters equal the ratio between the deviator stress increasing rather exponentially towards lower stress levels as illustrated in figure 4.15.

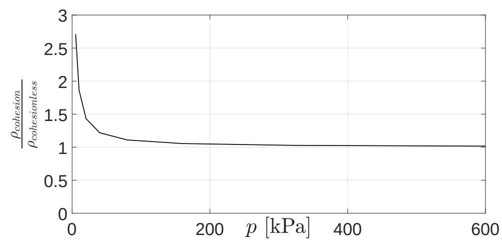

Figure 4.15: Significance of cohesion depending on stress level.

Implications on the stress-strain response when shifting to modified strength parameters are also elucidated through numerical soil tests seen in figure 4.16.

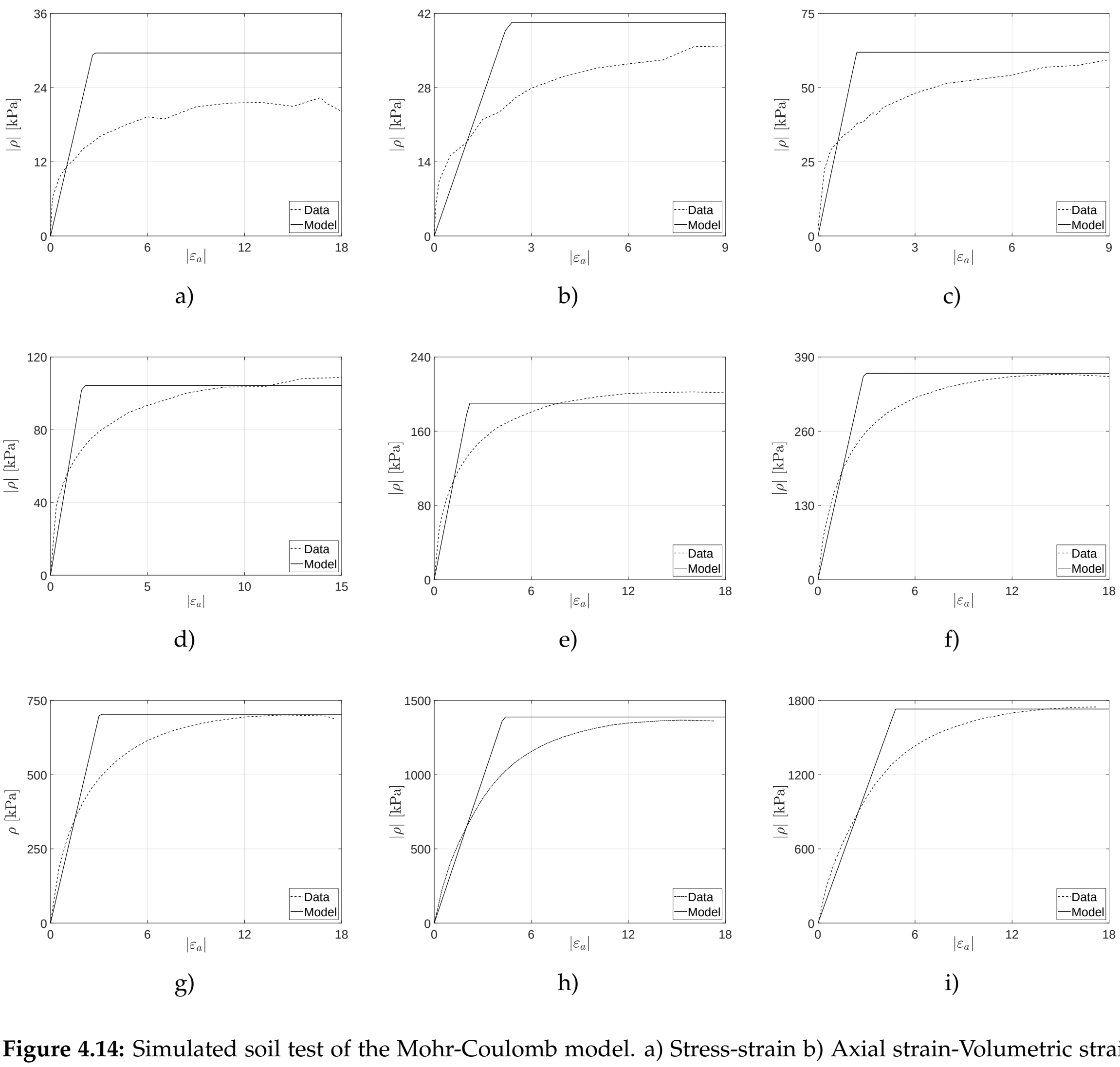

Figure 4.14: Simulated soil test of the Mohr-Coulomb model. a) Stress-strain b) Axial strain-Volumetric strain.

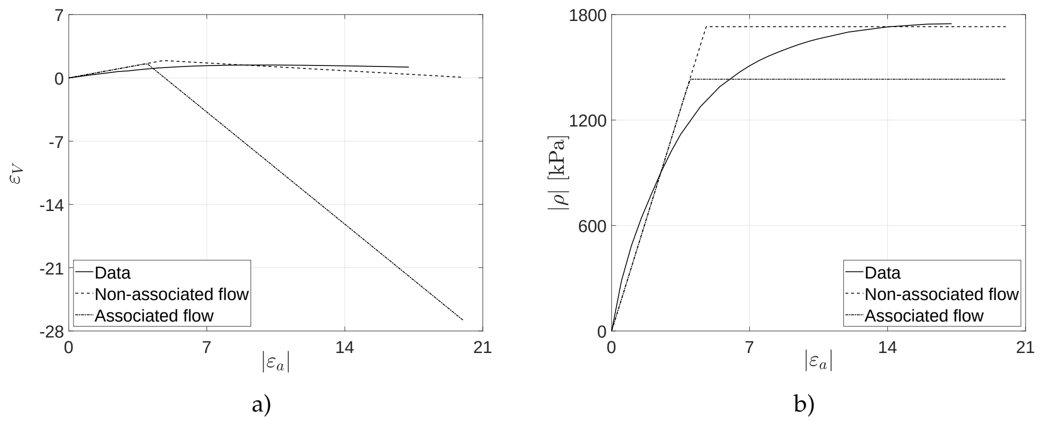

Figure 4.16: Simulated soil test of the Mohr-Coulomb model. a) Axial strain vs. volumetric strain b) Axial strain vs. deviator stress.

4.3.2 The General Parametric Model

Under the presumption that true triaxial test results are available the calibration procedure outlined in table 4.8 is recommended. It is clearly important to be aware of the test results a yield surface must be fitted to. Caution must be exerted in calibrating e.g. a Mohr-Coulomb setting of the general parametric yield surface from true triaxial test results. Even a slight change from a fully compressive triaxial state can discredit the use of a conventional fitting procedure and produce a yield surface on the unsafe side. The proposed procedure intuitively promotes a clear distinction between the stress states in a data set.

Table 4.8: Calibration procedure for the general parametric yield surface.

Iteration	Parameters	Data
1	φ', c'	$\sigma_1 = \sigma_2 > \sigma_3$
2	α	$\sigma_1 > \sigma_2 \approx \sigma_3$
3	β	$\sigma_1 > \sigma_2 > \sigma_3$

The procedure in table 4.8 is an iterative procedure with offset in a conventional fitting of Mohr-Coulomb to determine the friction angle and cohesion. The α parameter is then determined as a least squares fit with the two preceding parameters fixed. This is then repeated for β with the three preceding parameters fixed. Table 4.9 and figure 4.17 illustrates the procedure for loose G-12 sand.

Table 4.9: Calibration procedure for the general parametric yield surface for loose G-12 sand

Iteration	φ'	c'	α	β
1	31.50	0.76	0	10^{-4}
2	31.50	0.76	0.26	10^{-4}
3	31.50	0.76	0.26	0.08

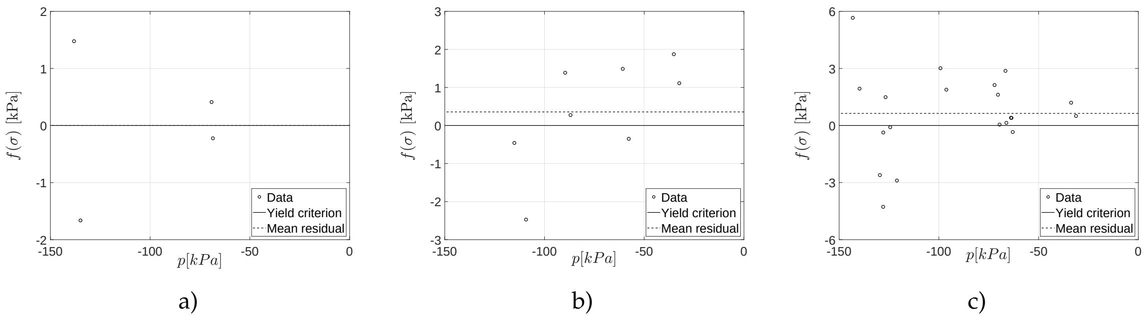

Figure 4.17: Steps in calibration procedure, loose G-12 sand. a) Iteration 1 b) Iteration 2 c) Iteration 3

This calibration is performed on both the loose, medium and dense sediments. The resulting parameters are shown in table 4.10 and the residuals are shown in figure 4.18 .

Table 4.10: Boending Parameters

I_D	φ'	c'	α	β
Loose	31.50	0.76	0.26	0.08
Medium	36.22	0.04	0.28	0.48
Dense	40.67	2.84	0.25	0.81

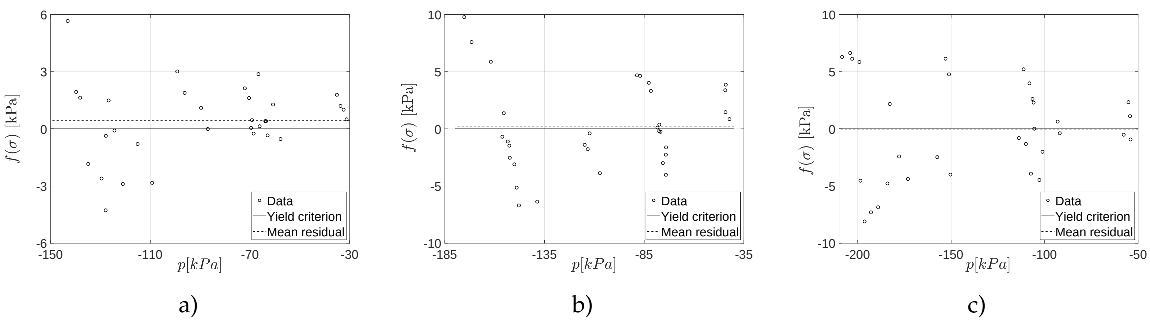

Figure 4.18: Residual plots of yield function for a) loose b) medium c) dense.

The fittingness of the parameters obtained from this calibration procedure is evaluated in table 4.11. Generally the higher stress levels tend to deviate more from the yield criterion numerically. Relative to the hydrostatic stress the deviations are though continuously in the same order of magnitude.

Table 4.11: Evaluation of calibrations. All values in [kPa].

G-12 sand, iterative	Loose	Medium	Dense
$\overline{f(\sigma)} = \frac{1}{N}\sum_{i=1}^{N} f(\sigma_i)$	0.429	0.168	-0.096
$\sigma = \sqrt{\frac{1}{N}\sum_{i=1}^{N}(f(\sigma_i) - \overline{f(\sigma)})^2}$	1.953	3.908	4.333
$max(\lvert f(\sigma_i)\rvert)$	5.661	9.770	8.010

The calibration procedure incidentally also promotes the use of the general parametric yield surface, even if true triaxial tests are not available. If only conventional compressive triaxial test results are available, the calibration is simply the first iteration. Likewise if only fully compressive/extensive triaxial test were conducted the first and second iteration can be applied.

Due to the novelty of the yield surface format, there is limited resources for benchmarking the proposed procedure. To assess the parameters, a comparison is made to those obtained in [25]. This calibration was performed on the exact same set of data. The parameters and fittingness can be reviewed in tables 4.12 and 4.13.

Table 4.12: Parameters for general parametric yield surface from [25]

I_D	φ'	c'	α	β
Loose	30.50	2.94	0.19	0.13
Medium	36.90	0.91	0.12	0.62
Dense	41.40	3.92	0.15	0.88

Table 4.13: Benchmark, deviation from table 4.11 shown in brackets. All values in [kPa].

G-12 sand, [25]	Loose		Medium		Dense	
$\overline{f(\sigma)} = \frac{1}{N}\sum_{i=1}^{N} f(\sigma_i)$	0.350	(-0.073)	-11.036	(-11.204)	-24.821	(-24.725)
$\sigma = \sqrt{\frac{1}{N}\sum_{i=1}^{N}(f(\sigma_i) - \overline{f(\sigma)})^2}$	1.906	(-0.047)	5.775	(+1.867)	10.116	(+5.783)
$max(\lvert f(\sigma_i)\rvert)$	6.734	(+1.073)	22.151	(+12.381)	42.815	(+34.805)

There is a clear discrepancy between the two calibrations. By fitting the parameters to the appropriate stress states there is a significant increase in the accuracy of the yield surface. Furthermore the apparent cohesion in the sand is not as significant. This is likely due to the exclusion of stress states that are not fully compressive when calibrating the cohesion in the iterative procedure.

To check the functionality of the soil model implemented in PLAXIS a series of triaxial tests are simulated and compared with values from the standard Mohr-Coulomb model. The deviatoric stress at failure for an extensive, compressive and shear stress states respectively, can be seen in tables 5.8.

Table 4.14: Deviatoric stress for dense G-12 sand at failure from test simulations of the PLAXIS Mohr-Coulomb model and the General Parametric model in a Mohr-Coulomb setting. All values in [kPa].

Confining pressure	1	10	100	1000
Compressive triaxial test				
Mohr-Coulomb	13.879	42.898	333.084	3234.992
General Parametric	13.879	42.898	333.084	3234.950
Extensive triaxial test				
Mohr-Coulomb	3.286	10.155	78.850	765.796
General Parametric	3.289	10.155	78.850	765.796
Direct shear test				
Mohr-Coulomb	4.629	14.274	110.439	1073.763
General Parametric	4.608	14.238	110.437	1072.751

The models generally coincide, but there is an unresolved discrepancy in the dilative response in the extension test. This is illustrated for dense G-12 sand in figure 4.19. It is most likely an issue with the stress return in the tensile region of the user defined mode, although the deviatoric stresses are identical.

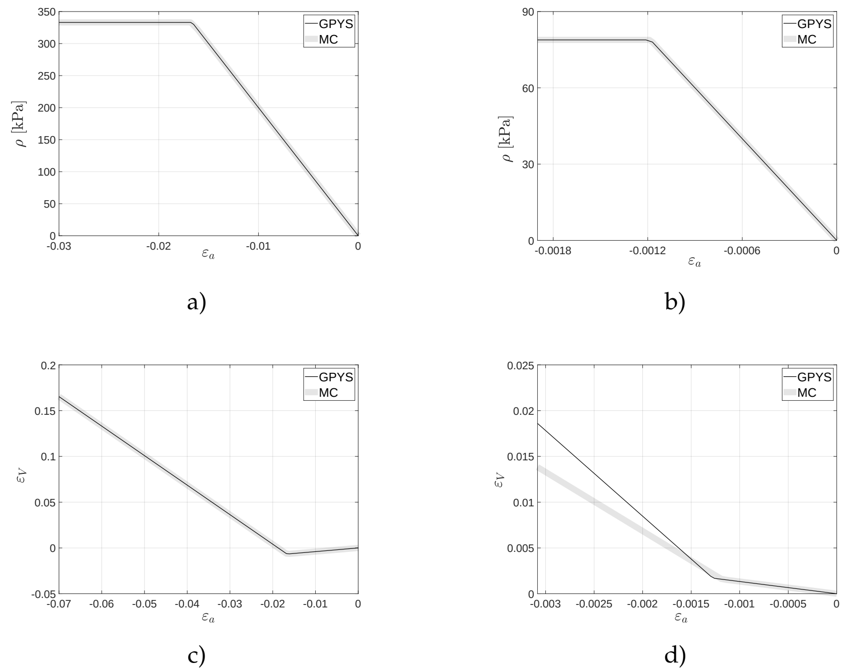

Figure 4.19: Axial strain vs. deviatoric stress and axial strain vs. volumetric strain at 100 kPa confining pressure.

Chapter 5

Analyses

In the following chapter different analyses of shallow foundations are performed and commented. Two- and three dimensional finite element models are generated in PLAXIS. The plane strain and axisymmetric assumptions are investigated with the Mohr-Coulomb model. The final section in the chapter presents analyses with the general parametric model implemented in PLAXIS. All analysis are performed on centrally loaded foundations at surface level with a fully saturated soil and a water head at the footing base level, as seen in figure 5.1.

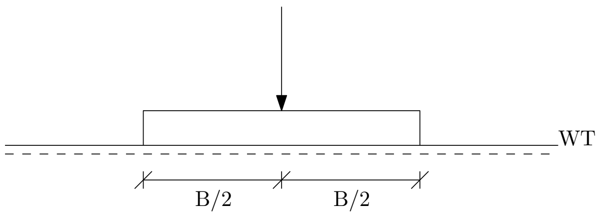

Figure 5.1: Centrally loaded foundation.

To facilitate a relatively large number of numerical analyses to be conducted in this thesis an alternative to operating PLAXIS through the graphical user interface is desired. Although PLAXIS is in essence reduced to a manageable amount of functionalities, compared to other finite element software such as e.g. Abaqus, setting up comparable models is still a time consuming task prone to mistakes and deviations. To avert this it is opted to write all analyses in scripts. In turn this increases efficiency and eases reproducibility. Another advantage is that analysis can be setup without necessarily having a PLAXIS license available on ones local machine and then run when convenient. Standalone scripts are written in Python, providing a recognisable and widely used coding language. The scripts are then passed through a remote scripting server, which has a special Python wrapper. In this manner the python scripts run as PLAXIS commands, ensuring exact reproduction for every simulation. It is also possible to write and run PLAXIS commands directly, but this is in the authors perspective a less elegant and intuitive "language". The primary tasks to be specified in the code are outlined in table 5.1. This is similar to a typical workflow in the graphical user interface, although not including any flow conditions. An example of a full script is included in appendix A.

Table 5.1: Primary tasks in PLAXIS.

Command in Python equivalent	Task
s_i.new	Start project
g_i.SoilContour	Define extend of soil domain
g_i.setproperties	Specify model/element type and units
g_i.soillayer	Define depth of soil layer
g_i.soilmat	Specify soil parameters
g_i.gotostructures	Define structures and loads/displacements
g_i.gotomesh	Define mesh
g_o.addcurvepoint	Preselection of nodes for data collection
g_i.gotostages	Define calculations phases
g_i.calculate	Calculate phases
g_i.view	See calculation results

To verify the plane strain and axisymmetric models analyzed, throughout the chapter, "ABC - Analysis of Bearing Capacity Version 1.0 Build 1" is used indicatively. This is a well-renowned solver to determine the ultimate bearing capacity of infinitely long strip footings and circular footings. It is based on the Mohr-Coulomb yield criteria and an associated flow rule. This is in line with majority of the finite elements models constructed in PLAXIS for this study. The three dimensional finite element code in PLAXIS is also deemed verified if the comparisons are acceptable. The program simply have 10 well-known user specified options, listed in table 5.2.

Table 5.2: User specified parameters/settings in "ABC".

Parameter/setting		Description
c0	[kPa]	Cohesion at footing level
k	[kPa/m]	Increase of cohesion with depth
φ	[^{o}]	Friction angle
γ	[kN/m^3]	Effective specific weight of soil
Strip		Plane strain analysis
Circular		Axisymmetric analysis
Smooth		Completely smooth soil-structure interface
Rough		Completely rough soil-structure interface
B	[m]	Width of strip footing or diameter of circular footing
q	[kPa]	Surcharge at footing level

5.1 The Assumption of a Infinitely Long Structure

When analysing a bearing capacity problem in plane strain the assumption is essentially an average solution which applies to the entire length of a structure. The structure is in principle considered infinitely long. This is a very effective and quite simple solution strategy. In danish geotechnical practice such problems are often solved with an increased friction angle, compared to that obtained from laboratory testing. It is of interest to investigate whether there are any potential pitfalls or untapped bearing capacity in relation to the full three dimensional structure. To initiate this study a series of three dimensional shallow foundations of altering width and length ratios are analysed. The material modelled is baskarp sand no. 15 for three different density indices. A principle sketch of the model is shown in figure 5.2 and the parameters are shown in table 5.3.

Table 5.3: Parameters for finite element model.

I_D	E_{ref}	E_{inc}	ν	c'	φ'	ψ	σ_t	γ	e_{init}
	[kPa]	[kPa]	[-]	[kPa]	[^{o}]	[^{o}]	[kPa]	[$^{kN}/_{m^3}$]	[-]
Loose	3752	413	0.30	4.64	28.01	28.01	0.00	18.86	0.85
Medium	9107	595	0.30	8.98	32.47	32.47	0.00	19.64	0.70
Dense	17186	653	0.30	12.99	36.00	36.00	0.00	20.16	0.61

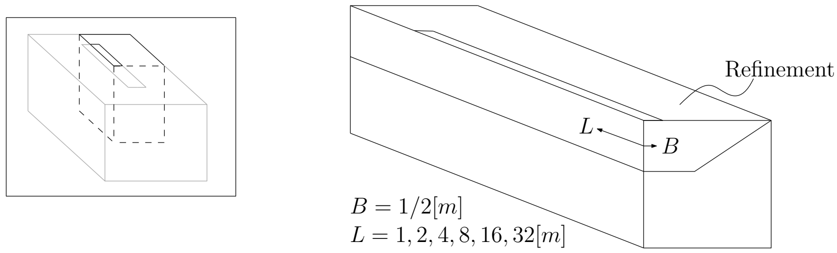

Figure 5.2: Principle sketch of finite element model.

The model exploits double symmetry, reducing the problem to a quarter of the full domain. To make the results comparable it is desired to keep the element size constant throughout all analyses. This is ensured by using a converged mesh as a benchmark and then generating the same element size for the altering domain size. This is controlled by the mesh value, denoted MV, as

$$MV = \frac{MV_{ref}\sqrt{l_{ref}^2 + w_{ref}^2 + d_{ref}^2}}{\sqrt{l^2 + w^2 + d^2}} \tag{5.1}$$

where l, w and d refer to the length, width and depth of the soil domain respectively. The averaged bearing capacity per unit area is plotted against the length of the foundation in figure 5.3.

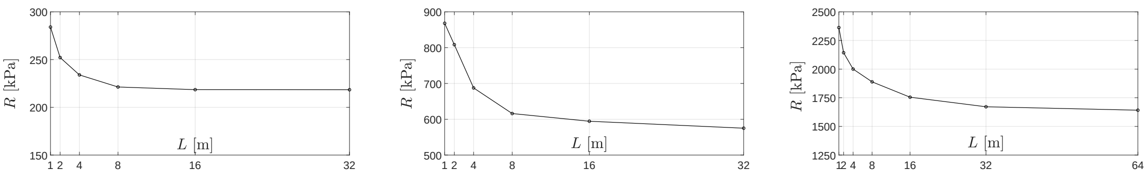

a) b) c)

Figure 5.3: Ultimate bearing capacity for a 1m wide strip footing with varying length for a) Loose b) Medium c) Dense.

These results imply that the average bearing capacity converges around a width to length ratio of 1:64. The averaged bearing capacity reduced with length. This is rather counter-intuitive in comparison to the the shape factors for the load bearing formulae presented in section 2.3.2. To take any possible size effects into account, similar analyses are performed for different widths of the foundation. The discrepancy between bearing capacity for different widths analysed with a width-length ratio of 1:32 and 1:64 respectively is seen in figure 5.4.

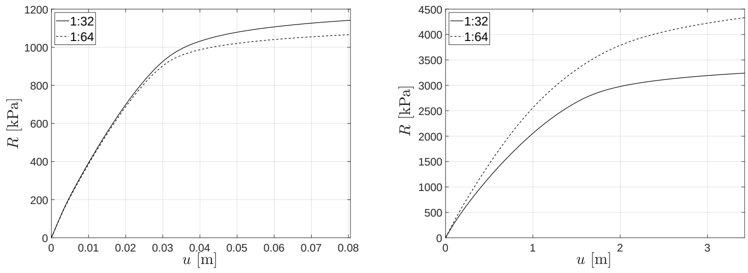

a) b)

Figure 5.4: Bearing capacity for a) 0.25m wide strip footing b) 5m wide strip footing.

It is evident that the width of the structure does influence how the bearing capacity develops with increasing length. Furthermore it is observed that the 1:64 ratio, for which the average bearing capacity is considered converged, result in a close to proportional relationship between width and bearing capacity. This ratio will be utilized for the three dimensional models to be compared with the plane strain analyses.

Plane friction angle

Using an increased friction angle in plane strain solution is widely accepted as good practice. The magnitude of the increase has been subject to change during the past decades, but generally limited to a maximum of 10%. Current practice prescribes that the increase is dependent on the density index of the soil. To get a first estimate of the magnitude of the discrepancy between plane strain and three dimensional solutions a number of generic models are analysed. Two plane strain solutions are obtained, one with an increased friction angle and one without. The increase is taken as 10% for all friction angles for the purposes of this investigation. As a side note this was, to the authors knowledge, historically, best practice for several years among practitioners. The parameters used for the models are stated in table 5.4 and the geometry is consistent with the previous study.

Table 5.4: Parameters for initial analyses.

	E	ν	c'	φ' & ψ	σ_t	γ	e_{init}
	[kPa]	[-]	[kPa]	[^{o}]	[kPa]	[kN/m^3]	[-]
Regular	15000	0.3	5	25, 30, 35, 40	0	20	0.6
Plane	15000	0.3	5	27.5, 33, 38.5, 44	0	20	0.6

The results of the generic examples are also used to verify the solution with "ABC" as seen in figure 5.5.

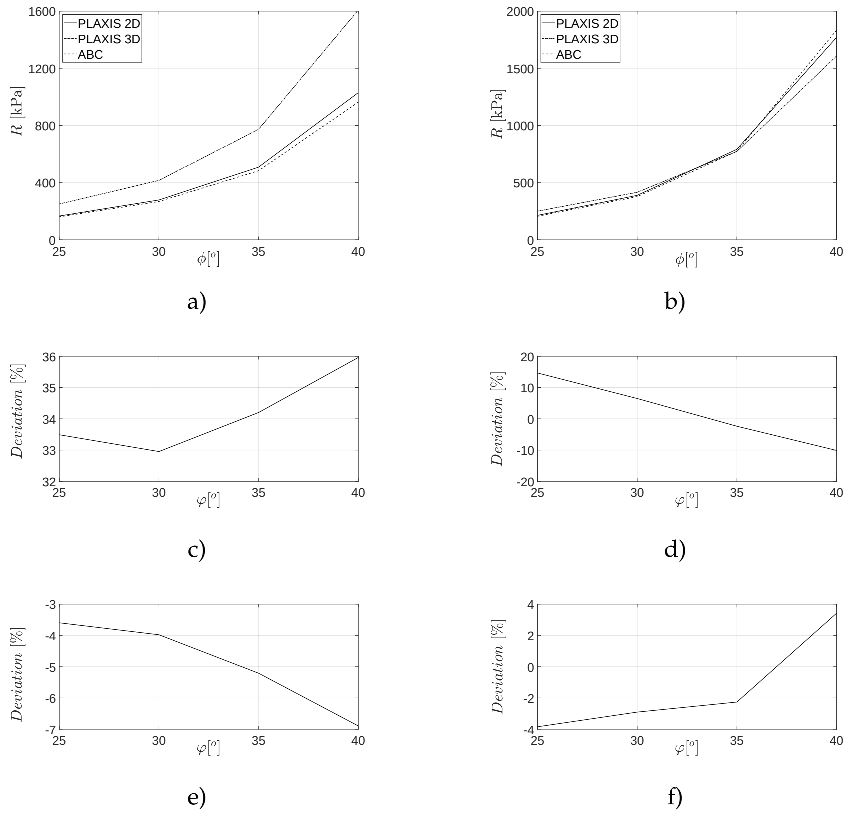

Figure 5.5: Friction angle against the ultimate bearing capacity for strip footings a) Regular friction angle b) Plane friction angle c) Deviation 2D-3D d) Deviation 2Dplane-3D e) Deviation 2D-ABC f) Deviation 2Dplane-ABC

As expected there is a clear difference between plane strain and three dimensional solutions. Furthermore the results show that the correction does reduce the discrepancy significantly. It also promotes the dependency on the density index, which in general is proportional to the friction angle.

To elucidate the implications of increasing the friction even further, a more comprehensive study is undertaken with the soil parameters from table 5.3. A series of plane strain analyses with altering dimensions and density indices are conducted. This is compared to identical cases analysed in three dimensional models. The difference between the plane strain analyses without any correction on the friction angle and the three dimensional analyses is shown in figure 5.6.

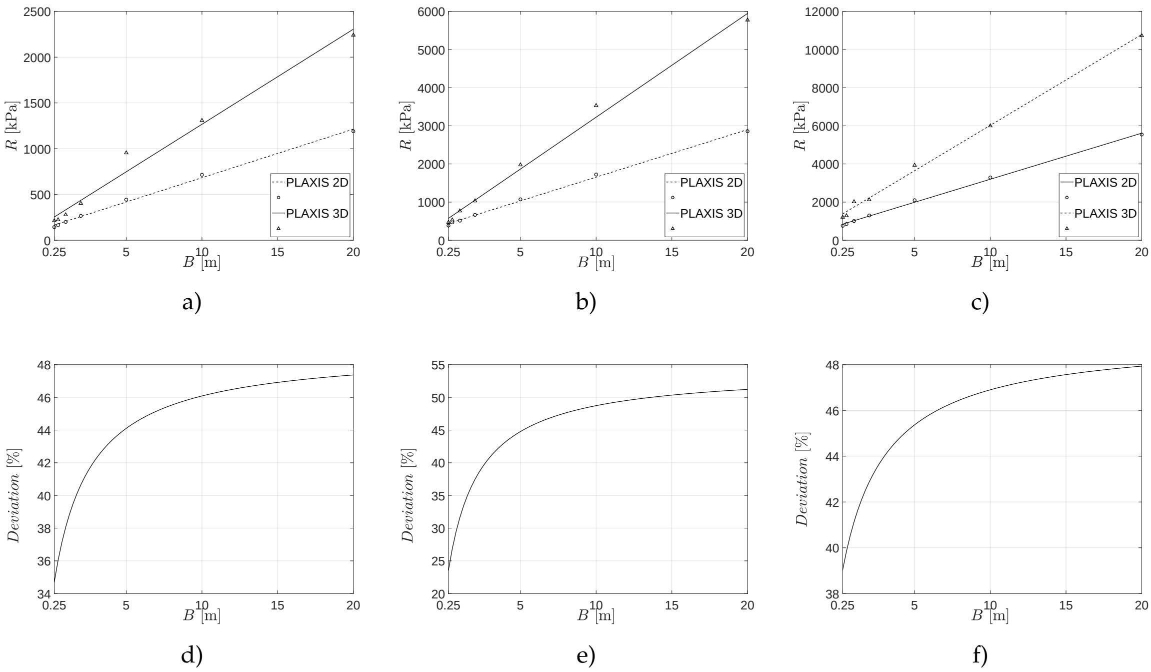

Figure 5.6: Ultimate bearing capacity for strip footings of varying size in PLAXIS 3D and PLAXIS 2D for a) loose b) medium c) dense.

Expectedly there is a significant difference in bearing capacity for all density indices and foundation sizes. The same problem is now analysed with corrected friction angles as in equation 2.6, which dependent on the density index and limited to a maximum increase of 10%. The difference in the angles is shown in table 5.5.

Table 5.5: Plane friction angles.

	Loose		Medium		Dense	
φ'	28.01		32.47		36.00	
φ'_{pl}	28.06	(+0.2%)	35.17	(+8.3%)	39.60	(+10%)

The increase on the loose sand is not of much practical interest. Analysis of a 1m strip footing reveals an increase in bearing capacity of merely 1.5% and no further analysis are executed for this sediment. It should be noted though that there is a significant deviation between the plane strain and three dimensional for this degree of compaction, so an increase would seemingly be justifiable. Bearing capacities for the medium and dense sands are presented in figure 5.7.

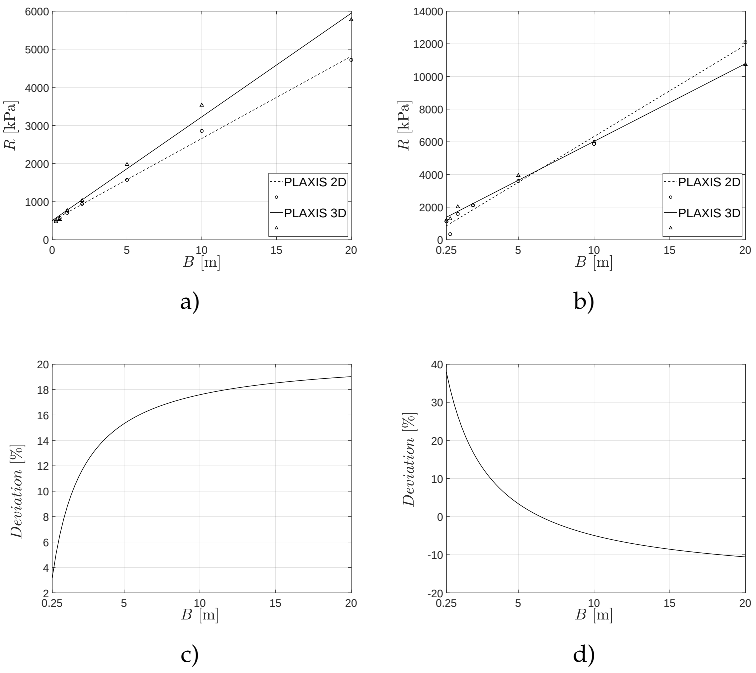

Figure 5.7: Ultimate bearing capacity for strip footings of varying size in PLAXIS 3D and PLAXIS 2D for a) medium b) dense.

The results for the dense sediments are quite contradictory to the observations in figure 5.6. This is likely owing to inconsistencies in the numerical models. For the medium sediments the bearing capacity from plane strain analysis with plane friction angle serves as a good approximation for the smaller foundation sizes, but deviates for the large which is consistent with the tendency in figure 5.6. Observing the general tendencies for the analyses conducted a correction of the friction angle dependent on both the density index and the size of the structure, could prove a feasible alternative to three dimensional analysis.

Comparison of solution strategies

The ultimate bearing capacity for all sizes investigated for the strip footing with the three density indices are depicted in figure 5.8 for varying widths. The analytical results are calculated using a plane friction angle and the numerical simulations are run with a triaxial friction angle.

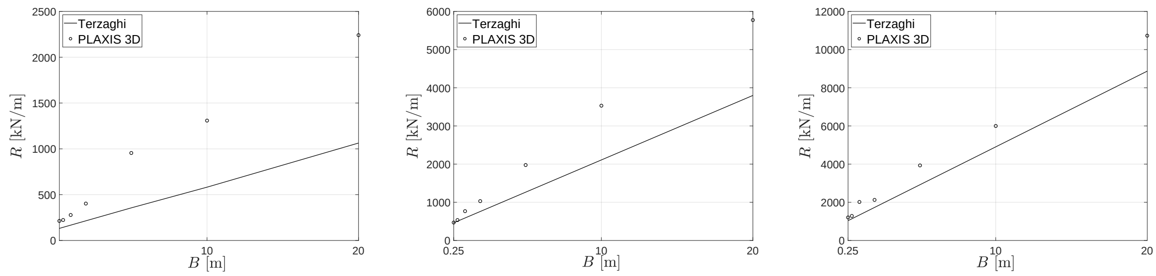

a) b) c)

Figure 5.8: Ultimate bearing capacity obtained from analytical results using Terzaghi and a plane friction angle, and numerical results for 3D models for a) loose b) medium c) dense.

The gain from running time consuming three dimensional analysis is evident and in today's practice the analytical approach is likely reduced to a first approximation at very early design stages. For all analyses performed it an estimate on the safe side, but caution should be exerted. For the medium sediment the values closely coincide for the small footings. As such there is no distinct trend promoting any further increases for the analytical approximate, even though it generally underestimates the bearing capacity.

5.2 Validity of Analyses Exploiting Rotational Symmetry

For circular footings the conventional method using bearing capacity formulae is to calculate a square with the same footprint area. In general square footings have a larger bearing capacity than circular footings as it might be on the unsafe side to do this. Furthermore, many times the plane friction angle is used even though analysing a circular footing is obviously not a plane problem, but a three-dimensional problem. This does though seem to generate overly conservative results, even if using non-associated parameters with a plane strain friction angle and hereby producing the most favourable conditions within the framework of the bearing capacity formulae considered best practice. This analysis seeks to investigate when these assumptions might become critical and which pitfalls should be avoided.

The models used in present analysis is obviously conducted on a case simulating a circular footing. This is modelled with varying radius, and solely one quarter of the circular foundation is modelled in three-dimensional models. The analysis is made deformation based. The investigation is performed with associated geotechnical parameters using the modified formulae on Baskarp sand and on Mohr-Coulomb soil. It is made for all the three types of relative indices: loose, medium and dense sand and the parameters for this analysis are presented in table 5.6.

Table 5.6: Parameters for finite element model.

I_D	E_{ref}	E_{inc}	ν	c'	φ'	ψ	σ_t	γ	e_{init}
	[kPa]	[kPa]	[-]	[kPa]	[^{o}]	[^{o}]	[kPa]	[$^{kN}/_{m^3}$]	[-]
Loose	3752	413	0.30	4.64	28.01	28.01	0.00	18.86	0.85
Medium	9107	595	0.30	8.98	32.47	32.47	0.00	19.64	0.70
Dense	17186	653	0.30	12.99	36.00	36.00	0.00	20.16	0.61

Generic examples on a circular footing with increasing friction angle

To initiate investigations, as to whether an increase in friction angle for axisymmetric solutions could be justifiable, a set of generic models are formed. The object is firstly to create an overview of the discrepancy between axisymmetric and three dimensional solutions. Secondly any proportionality with increase in friction angle is sought elucidated.

A circular footing of 1m in diameter in both axisymmetry and 3D is investigated to see the influence of increasing the friction angle and keeping all other parameters constant. The investigated friction angle span from 25-40^o with a interval of 5^o. Parameters used in this analyses are presented in table 5.7 and the models are set up as previously mentioned. To streamline the models and to have the same errors the models are made with the exact same elements, waterlevel, meshvalues and coarseness factors etc. If not specified the values in PLAXIS is set as the default settings or the parameter is not relevant to the results.

Table 5.7: Parameters for initial analyses.

E	ν	c'	φ' & ψ	σ_t	γ	e_{init}
[kPa]	[-]	[kPa]	[^{o}]	[kPa]	[$^{kN}/_{m^3}$]	[-]
15000	0.3	5	25, 30, 35, 40	0	20	0.6

Results of the generic example for the 1m diameter circular footing is depicted in figure 5.9 showing the increase of the ultimate bearing capacity when increasing the friction angle.

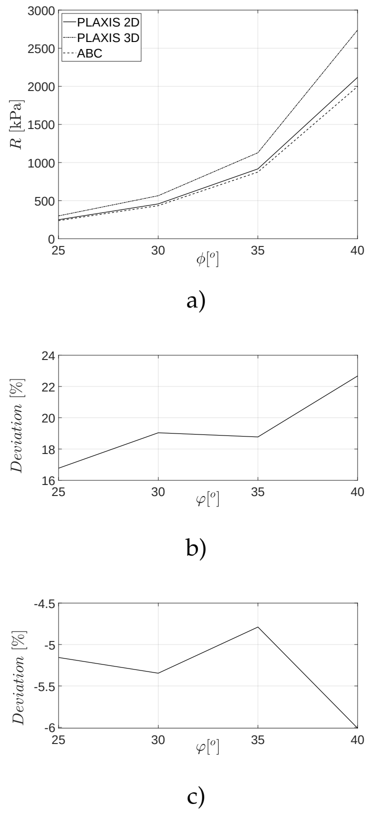

Figure 5.9: Friction angle against the ultimate bearing capacity for a circular footing showing a) Bearing capcities b) Deviation between axisymmetry and three-dimensional c) Axisymmetry against ABC results.

Results of the generic examples shows a fairly good relation between analysing a circular footing using axisymmetry and three-dimensional models. As expected the three-dimensional results are much higher than the axisymmetric.

Size effects on circular footings

In this analysis the ultimate bearing capacity for varying diameters is investigated. This is investigated in both PLAXIS 2D and 3D for the different density indices. The ultimate bearing capacities for circular footings at different sizes along with the deviations are presented in figure 5.10.

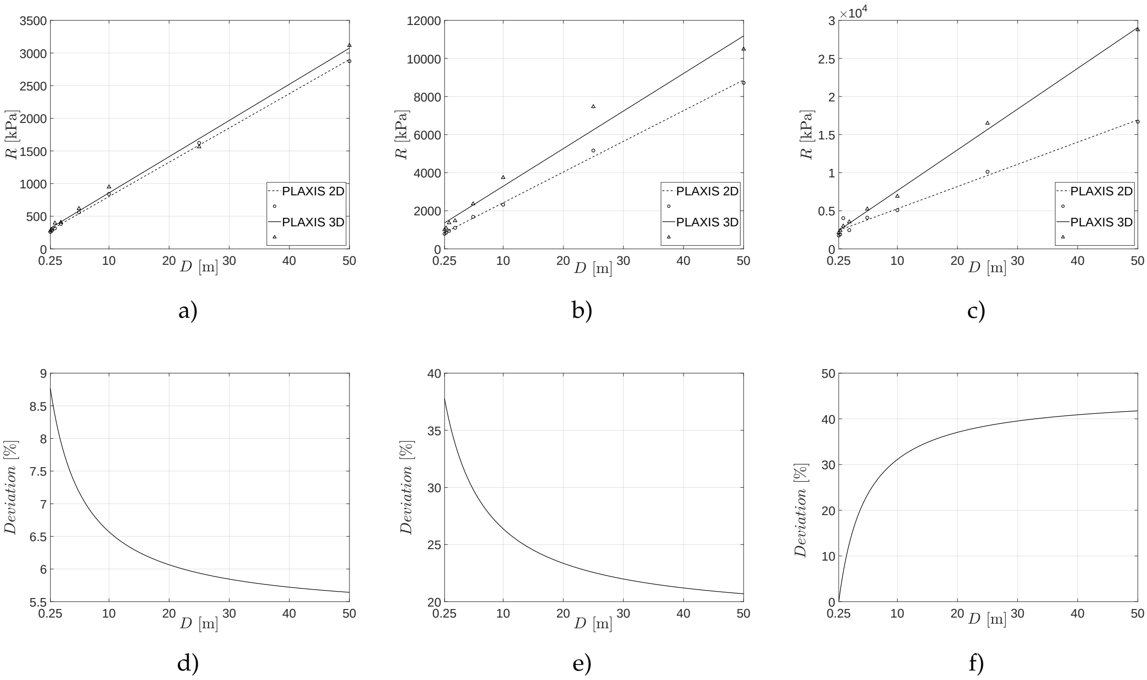

Figure 5.10: Size effects circualr footing. a) Loose b) Medium c) Dense

A larger load at failure is expected for the 3D models cf. the generic example, and also this investigation prepare the ground for correcting a parameter, which could be the friction angle, as for plane strain, in axisymmetry to attain a higher ultimate bearing capacity in axisymmetric calculations. This investigation also shows, that the ultimate bearing capacity is not proportional, but more exponential with the friction angle. The results show that the 2D are conservative and that a modification will be a good idea.

Comparison of solution strategies

It is very much used in danish geotechnical practice to convert a circular footing into an equivalent square footing of same area and use Terzaghi's bearing capacity formulae to give a first guess on the necessary size of the footing. The use of this is compared to numerical results conducted from PLAXIS 2D and 3D respectively. Numerically the calculation methods when analysing a circular footing in axisymmetry and three-dimensions are very different. This investigation is thus made on a 3D model and an axisymmetric model in the conventional program PLAXIS to invetigate the difference. Also gains from conducting a three-dimensional model versus solely an axisymmetric model are investigated.

However, also in the circular footing the cohesion is used in the analytical calculations to have the best frame of reference to the numerical results as these also utilizes cohesion. The deviation for all sizes investigated for the three density indices are depicted in figure 5.11.

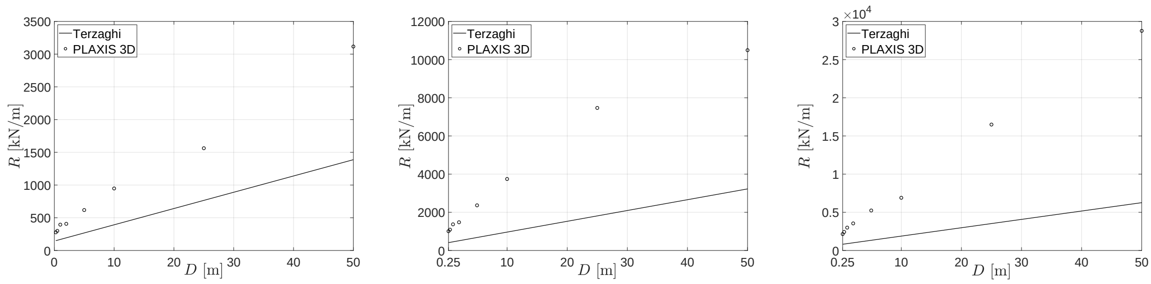

a) b) c)

Figure 5.11: Ultimate bearing capacity obtained from analytical results using Terzaghi and numerical results for 3D models for a) loose b) medium c) dense.

5.3 Gain from Approaching a Accurate Yield Surface

The implications of the new yield surface is firstly illustrated at a stress point level. The increase in deviatoric stresses for different stress states is shown in 5.8

Table 5.8: Deviatoric stress for dense G-12 sand at failure from test simulations of the PLAXIS Mohr-Coulomb model and the General Parametric model with appropriate α and β parameters.

Confining pressure	**1**	**10**	**100**	**1000**
Compressive triaxial test				
Mohr-Coulomb	13.879	42.898	333.084	3234.992
General Parametric	13.879	42.898	333.084	3234.950
Extensive triaxial test				
Mohr-Coulomb	3.286	10.155	78.850	765.796
General Parametric	3.593	11.104	86.220	837.379
Direct shear test				
Mohr-Coulomb	4.629	14.274	110.439	1073.763
General Parametric	5.285	16.336	126.840	1231.916

To verify that the General Parametric model implemented in PLAXIS provides credible results, an example from [25] is used as benchmark. It should be noted that the result is prone to errors due to differences between the finite element codes, iterative methods and user defined models. The load-displacement response can be seen in figure 5.12

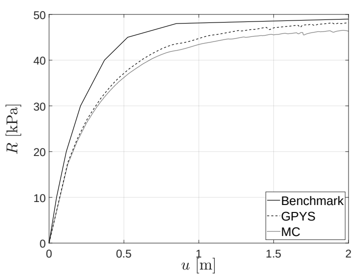

Figure 5.12: Load-displacement response of 0.4 x 0.4 m pad foundation.

There is a 1.67% deviation on the ultimate bearing capacity, which is deemed acceptable owing to the sources of error stated before. The displacement response is much stiffer in the benchmark solution and the user defined soil model undoubtedly needs more rigorous verification on some key features, such as the stress return.

A three dimensional 1m x 64m strip footing is analysed to illustrate the potential gain of increasing the accuracy of the yield criteria in non-linear finite element analysis. All the material parameters used in the analysis in present section are summarized in table 5.10.

Table 5.9: Parameters for finite element model.

I_D	E	ν	c'	φ'	ψ	γ	e_{init}	α	β	β_t
	[kPa]	[-]	[kPa]	[^{o}]	[^{o}]	[$^{kN}/_{m^3}$]	[-]	[-]	[-]	[-]
Loose	5000	0.30	0.666	28.29	28.29	19.37	0.75	0.26	0.08	0
Medium	12000	0.30	0.036	33.59	33.59	20.12	0.62	0.28	0.48	0
Dense	20000	0.30	2.592	38.11	38.11	20.58	0.55	0.25	0.81	0

The difference between the ultimate bearing capacities is shown in table 5.10.

Table 5.10: Ultimate bearing capacities. All values in [kPa]

	Loose		**Medium**		**Dense**	
Mohr-Coulomb	261.1		325.7		850.1	
General Parametric, $\beta = 0$	263.2	(+0.8%)	337.9	(+3.8%)	930.8	(+9.5%)
General Parametric	263.5	(+0.9%)	352.3	(+8.2%)	1001.5	(+17.8%)

There is certainly a large potential gain in bearing for especially dense sediments, by implementing more accurate material models. To properly quantify the potential increase further study is needed.

Chapter 6

Conclusion

The purpose of this study is to elucidate potential pitfalls or gains in elasto-plastic finite element solutions of geotechnical problems. The two main focuses are the coherence between two- and three dimensionality, and the accuracy of the constitutive modelling involved in formulating problems for shallow foundations in the ultimate limit state. In spite of the computer power available today, large three dimensional finite element models are still time-consuming to solve, even for problems as seemingly simplistic as the ones analysed in this thesis. Thus facilitating better two-dimensional approximation is of interest, especially for practitioners working on tight schedules. This leads to the premise, as to whether best practice in geotechnical industry is really suitable for transitioning into even more numerical analysis. Firstly the correction of the friction angle, when treating problems in plane strain is investigated. This leads to the question as to whether something similar could be justified for axisymmetric analysis.

The plane strain analyses performed on altering sizes of strip foundations are compared to equivalent three dimensional analyses. The results clearly validate the use of some correction to increase the bearing capacity of the plane strain case. The study is by no means exhaustive, but quite unambiguously reveal a trend for the difference between two- and three dimensional analyses to be size dependent. Besides this it discredits the possible conservatism of very low increases at low density indices. This being said the bearing capacity is not linearly dependent on the friction angle, but the expression for correcting the friction angle is. A non-linear expression dependent on the density index and size of the structure could prove a good solution, but a formulation was not reached in this thesis.

The axisymmetric analyses were also performed on varying sized structures and with different density indices. Much like in the plane strain case, there were trends of significant discrepancies between the analysis types. Unfortunately the tendencies where not clear-cut, due inconsistencies in the numerical models. The authors do believe there is a potential in investigating the relation further, but cannot currently quantify anything specific.

The general parametric yield surface shows great promises of being a substitute or addition to the Mohr-Coulomb criterion in commercial geotechnical software for a number of reasons. The more obvious is that it can emulate Mohr-Coulomb, so that nothing would be lost in this regard. Furthermore the simplicity in its formulation and clear physical interpretation of the parameters will most likely appeal to many practitioners. The versatility of the criteria will likely mean that it can replace a number of criteria. In the authors perspective this could also promote more familiarity and physical understanding when using numerous yield criteria in ones day to day routines. There is undoubtedly also a justifiable increase in strength. This could possibly be exploited even further in combination with advances in structures manipulating the stresses to more prudent stress states or levels. Although not rigorously checked for its performance in numerical analysis for the purposes of this study, the General Parametric model was at a first glance deemed on par with the standard models implemented in PLAXIS.

Bibliography

[1] DS/EN 1997-1 DK NA. *DS/EN 1997-1 DK NA:2015 - Nationalt Anneks*. Dansk Standard. 2015.

[2] Andersen J. D., Fuglsang L. D., Christensen H. F., Nissen R. W., Augustesen A. H., Thøgersen L., ..., Galsgaard J. *Eksempelsamling til Lærebog i Geoteknik*. dgf-Bulletin 22. Dansk Geoteknisk Forening, 2010.

[3] Ovesen N. K., Fuglsang L. D., Bagge G. & Krogsbøll A. *Lærebog i Geoteknik*. 2nd ed. Polyteknisk Forlag, 2014.

[4] Ottosen N. S. & Ristinmaa M. *The Mechanics of Constitutive Modelling*. Elsevier Ltd., 2005.

[5] Bønding N. *Bulletin No. 30, Triaxial State of Failure in Sand*. The Danish Geotechnical Institute. 1977.

[6] Bødker L. & Ibsen L. B. *Baskarp Sand No. 15, data report 9301*. Aalborg University. 1994.

[7] PLAXIS. *PLAXIS 3D Reference Manual*. V20. 2018.

[8] Yu H. *Plasticity and Geotechnics*. 2nd ed. Springer Science+Business Media, LCC, 2006.

[9] PLAXIS. *PLAXIS 3D Material Models Manual*. V20. 2018.

[10] DS/EN 1997-1 DK NA. *DS/EN 1997-1:2007 Geoteknik - Del 1: Generelle regler*. European Comitee for Standardization (CEN). 2007.

[11] Clausen J., Damkilde L. & Krabbenhoft S. "The Bearing Capacity of Circular Footings in Sand: Comparison between Model Tests and Numerical Simulations Based on a Nonlinear Mohr Failure Envelope". In: *Advances in Civil Engineering* (2012), p. 10.

[12] Hicher P. & Shao J. *Constitutive Modeling of Soil and Rock*. ISTE Ltd and John Wiley & Sons, Inc., 2008.

[13] Maranha J. R. & Maranha das Neves E. *The experimental determination of the angle of dilatancy in soils*. 2009.

[14] Potts D. M. & Zdravkovic L. *Finite element analysis in geotechnical engineering, Theory*. Thomas Telford Publishing, 1999.

[15] Damkilde L., Krabbenhoft K. & Krabbenhoft S. *A contribution to a new bearing capacity equation in cohesionless soil*. Department of Civil Engineering, Aalborg University, Esbjerg, Denmark & School of Engineering, University of Liverpool, UK. 2019.

[16] Oberhollenzer S., Schweiger F. H. & Tschuchnigg F. "Finite element analyses of slope stability problems using non-associated plsaticity". In: *Journal of Rock Mechanics and Geotechnical Engineering* 10 (2018).

[17] Terzaghi K. *Erdbaumechanik auf bodenphysikalischer Grundlage*. 1925.

[18] Kelly. *Solid Mechanics Part II: Engineering Solid Mechanics – small strain*. 28. URL: \http://homepages.engineering.auckland.ac.nz/\~pkel015/SolidMechanicsBooks/Part_II/index.html.

[19] Martin C. *User Guide for ABC – Analysis of Bearing Capacity Version 1.0*. Department of Engineering Science, University of Oxford. 2004.

[20] *Foundations*.

[21] Martin C. *Exact bearing capacity factors for strip footing. Downloads - Bearing capacity factors*. 2005. URL: \http://www2.eng.ox.ac.uk/civil/people/cmm.

[22] Islam M. S., Rokonuzzaman M. & Sakai T. "Shape Effect of Square and Circular Footing under Vertical Loading: Experimental and Numerical Studies". In: *International Journal of Geomechanics,* (2017).

[23] PLAXIS. *PLAXIS Scientific Manual*. V20. 2017.

[24] Al-Aukaily A. & Scott M. H. "Sensitivity Analysis for Displacement-Controlled Finite-Element Analyses". In: *Journal of Structural Engineering, ASCE* (2017).

[25] Nielsen J. & Jepsen K. S. "Elasto-Plastic Constitutive Modelling of Geotechnical Material". MA thesis. Aalborg University, Esbjerg, 2019.

[26] Azizi F. *Applied Analyses in Geotechnics*. E & FN Spon, 2000.

Appendices

Appendix A

Python Editor Example for PLAXIS 3D

It is very feasible to use Python Editor when analysing geotechnical structures in PLAXIS as the risk of mistakes is much smaller than if using the graphical user interface. The Python Editor is used along with the student version and the analyses are based on python coding implemented in PLAXIS. The python code is programmed in Python Editor for PLAXIS 2D and 3D. Several structures are made in PLAXIS and force-deformation analyses are run. Structures simulating circular and strip footings are analysed during the project. The python scripts are made for convenience when editing a structure or parameter in the numerical model. In this chapter the procedure of setting up a python code for a circular footing in 3D is described. If not specified, the default settings of PLAXIS is used.

Connecting to PLAXIS application and starting a new project to get the Python Editor to run properly. If you have a licence from Aalborg University use CodeMeter Control Center to activate the license. Open PLAXIS 2D Input or PLAXIS 3D Input depending on, what you are about to model. Go to "Expert" in the top menu and then go to "Configure remote scripting server". Here, an available server port should be chosen. Most often port 10000 and 10001 is chosen, which are the default ports in PLAXIS. The ports are imported by the "localhostport" command. Note that it begins with node zero (10000). In the "Configure remote scripting server" window a user specific code is presented as well. The path of the scripting libraries are defined and afterwards imported. Now, it is possible to connect to PLAXIS by the commands used in table A.1 to define the server and start a new project.

Table A.1: Connecting to PLAXIS application and starting a new project.

Connecting to PLAXIS

```
localhostport = 10000
localhostport_output = 10001

pswrd='12345789'

plaxis_path=r'C\:\Program Files\Plaxis\PLAXIS 3D\python\Lib\site-packages'

import imp
found_module = imp.find\_module('plxscripting', [plaxis\_path])
plxscripting=imp.load\_module('plxscripting', *found\_module)
from plxscripting.easy import *
import math

s_i,g_i=new_server('localhost',localhostport,password=pswrd)
s_o,g_o=new_server('localhost',localhostport_output,password=pswrd)

s_i.new()
```

General inputs and project properties are now implemented in the python code by using the commands in table A.2. The radius of the circular footing and the geometry of the model domain is defined. The model domain is defined in the xy-plane using "SoilContour". The general project properties are defined by the type of model and elements. The model is either a full (3D) or axisymmetric/plane strain (2D) model. The element type used for 3D models is 10-noded and 15-noded elements for 2D models. The units used in the code are defined as well.

Table A.2: Defining general inputs and project properties.

General inputs and project properties

```
b=50
X1, Y1, Z1, X2, Y2, Z2, X3, Y3, Z3, X4, Y4, Z4 = 0, 0, 0, 0, 5*b, 0, 5*b, 5*b,
0, 5*b, 0, 0
Xmin=0
Ymin=0
Xmax=5*b
Ymax=5*b
g_i.SoilContour.initializerectangular (Xmin,Ymin,Xmax,Ymax)
g_i.setproperties("ModelType","Full","ElementType","10-Noded","UnitForce","kN",
                  "UnitLength","m","UnitTime","s")
```

Afterwards, the borehole is created and the depth of the layer and the water head are defined as well.

Table A.3: Creating borehole.

Borehole

```
D_bottom = 5*b
H_ref = 0

borehole = g_i.borehole(0,0)
g_i.soillayer(D_bottom)
borehole.setproperties("Head",H_ref)
```

Defining soil material by connecting a material model to the soil material by the "soilmodel" command. PLAXIS recommend three material models for gravel and sandy soils. Mohr-Coulomb is one of the recommended models, and the two alternavitives are based on Mohr-Coulomb, hence solely this is used from PLAXIS in present project. Mohr-Coulomb is the second material model in PLAXIS, hence 2 is used as the soil model. The two alternative models are better at calculating deformations and liquefied soils, hence they are not relevant for present project. For further explanation of the models see (citePLAXISmanual-2D-3-Material-models). Additionally, a user-defined material model is implemented in PLAXIS, as described in section 3. This is implemented in the Python Editor by using soil model 16, which stands for user-defined. The parameters of the soil material are defined as well, see table A.4.

Table A.4: Creating the soil material.

Creting soil material

```
soilmodel = 2
gammaunsat = 16.36
gammasat = 20.16
nu = 0.3
Emodu = 17186
Einc = 653
yref = 0
Gmodu = Emodu/(2*(1+nu))
Ginc = Einc/(2*(1+nu))
c = 12.99
phi = 36
psi = 36
k_x = 0.001
k_y = 0.001
```

Importing the defined soil material to the layer by using the commands presented in table A.5.

Table A.5: Defining the soil material.

Defining soil material

`material = g \_i.soilmat()`
`material.setproperties("MaterialName", "Sand" ,`
`"Colour", 964844 ,`
`"SoilModel" ,soilmodel,`
`"gammaUnsat", gammaunsat,`
`"gammaSat", gammasat,`
`"Gref", Gmodu,`
`"Ginc", Ginc,`
`"nu", nu,`
`"cref", c,`
`"phi", phi,`
`"psi", psi)`
`material.setproperties("perm_primary_horizontal_axis", k_x ,`
`"perm_vertical_axis", k_y )`
`material.setproperties("FlowDataModel" , 200 ,`
`"HydraulicModel" , 1,`
`"DataSetFlow", 2,`
`"UsdaSoilType", 0,`
`"DefaultValuesFlow", True)`
 	
`g_i.Soils[0].Material = material`

A prescribed displacement is used to find the load and displacement at failure, hence the prescribed displacement must be chosen high enough to find these. A polyline is created and a surface within the circumference is defined. A surface displacement is put on the surface with a prescribed displacement in the z direction and no freedom to move in the x and y direction as these are fixed. The commands are presented in table A.6.

Table A.6: Defining a prescribed displacement.

Prescribed displacement

`g_i.polycurve((0,0,0),(1,0,0),(0,1,0),"line",0,b/2,"arc",90,90,b/2,"line",90,b/2)`
`g_i.surface(g_i.Polycurve_1)`
 	
`g_i.surfdispl(g_i.Surface_1)`
 	
`g_i.SurfaceDisplacement_1.Displacement_x="Fixed"`
`g_i.SurfaceDisplacement_1.Displacement_y="Fixed"`
`g_i.SurfaceDisplacement_1.Displacement_z="Prescribed"`
`g_i.SurfaceDisplacement_1.uz=-0.5`

Mesh refinement is applied to the model by a mesh value and coarseness factors. A new polyline almost at the edge of the surface is created. A coarseness factor is added to the line with regard to mesh refinement. The smaller the coarseness factor, the finer the mesh. A mesh value is used for the rest of the soil layer in the soil volume. If more lines were added these could have another coarseness factor. The commands are presented in table A.7.

Table A.7: Defining mesh refinement.

Mesh refinement
`g_i.polycurve((b/2+0.01,0,0),(1,0,0),(0,1,0),"arc",90,90,b/2+0.01)`
`CF=0.03125`
`MeshValue=0.10`
`g_i.gotomesh()`
`g_i.Polycurve_2_1.setproperties("CoarsenessFactor", CF)`
`g_i.mesh(MeshValue)`

Preselection of a node for calculation is chosen for the calculations by use of the "add-curvepoint" command presented in table A.8. Remember to add the node in the correct soil volume and layer, if multiple layers are defined.

Table A.8: Preselection of node for calculation

Preselection of node
`X_o=b/2`
`Y_o=0`
`Z_o=0`
`g_i.selectmeshpoints()`
`g_o.addcurvepoint(node, g_o.Soil_1_1, (X_o, Y_o, Z_o))`
`g_o.update()`

Staged construction is defined by different phases in attempt to calculate the ultimate bearing capacity, see table A.9. Firstly, an initial phase is automatically generated. Afterwards, the first phase is generated. This is where the displacement is activated and established. The deformation type is very important. Here, it is a plastic deformation type. Some of the things, that are easily changed if the calculation is not run properly is the maximum steps and the tolerated error. For both parameters the accuracy of these applies. They should not be to high as the calculation time may be to long considering what is gained. On the other hand it should not be too low as the error might be too high. Thus, it needs to be high enough to run a proper analysis.

Table A.9: Staged construction.

Staged construction
`g_i.gotostages()`
`g_i.phase(g_i.InitialPhase)`
`g_i.setcurrentphase(g_i.Phase_1)`
`g_i.Phase_1.Identification="Installation"`
`g_i.Phase_1.DeformCalcType="Plastic"`
`g_i.Phase_1.Deform.UseDefaultIterationParams=False`
`g_i.Phase_1.Deform.MaxSteps=10000`
`g_i.Phase_1.Deform.ToleratedError=0.01`
`g_i.Phase_1.Deform.MaxIterations=60`
`g_i.Phase_1.Deform.MaxUnloadingSteps=15`
`g_i.SurfaceDisplacement_1.activate(g_i.Phase_1)`

Calculate and view results by using the commands in table A.10. PLAXIS 3D Output is autoatically opened when using the "view"command. The phases are now calculated and the results from the selected node can be extracted from the output window.

Table A.10: Calculate and view results.

Calculate and view results
`g_i.calculate()`
`g_i.view(g_i.Phase_1)`

Extract results from PLAXIS Output e.g. a force-displacement curve. To extract this one must open PLAXIS Output and go to "Curve Manager" in the top menu. In the curve manager the node is chosen as one of the xx and the project as the other. Afterwards the force in the specific direction and the displacement in the same direction is chosen.